Available online at www.sciencedirect.com
SCIENCE DIRECT®
Tectonophysics 364 (2003) 85–113
TECTONOPHYSICS
www.elsevier.com/locate/tecto

Kinematic and structural development of the Çankiri Basin (Central Anatolia, Turkey): a paleostress inversion study

Nuretdin Kaymakci[a,*], Stanley H. White[b], Paul M. Vandijk[c]

[a] *Geological Engineering Department, Faculty of Engineering, Middle East Technical University, 06531-Ankara, Turkey*
[b] *Faculty of Earth Sciences, Utrecht University, Budapestlaan 4, 3508 Utrecht, The Netherlands*
[c] *ITC Hengelosestr 99, P.O. Box 6, 7500 AA Enschede, The Netherlands*

Received 13 November 2002; accepted 23 January 2003

Abstract

Three different deformation phases have been recognized in the southern part of the Çankırı Basin from (1) the major structures and (2) through using paleostress inversion techniques for fault slip data. The deformation phases recognized from the paleostress data are correlated with those recognized from the major structures and dated accordingly. The first phase occurred in the Late Paleocene to pre-Burdigalian and is characterized by an oblique σ_2 and NNE–SSW to NE–SW trending subhorizontal σ_1 and WNW–ESE to NW–SE trending σ_3 patterns which indicate transcurrent deformation associated with a combination of thrusting and strike slip faulting (transpression) possibly due to indentation of the Kırşehir Block to the Sakarya Continent. The second phase occurred from the Burdigalian to the Serravallian and is characterized by a subvertical σ_1 and oblique σ_2 and σ_3, which indicate oblique extension associated with normal faulting possibly due to a post-orogenic collapse. The third deformation phase is characterized by a vertical σ_2 while the other stresses were horizontal, which indicate regional transcurrent tectonics, which is correlated with the current transcurrent tectonics controlled by the North Anatolian Fault Zone.

Keywords: Paleostress inversion; Çankırı; Kinematics; Transcurrent; Turkey

1. Introduction

Paleostress inversion methods provide an estimation of the orientation of the principal stress axes using fault slip data sets. The direction of slip is inferred from the fault slip data, which are assumed to record the direction of maximum shear stress on a fault surface (Carey and Brunier, 1974; Etchecopar et al., 1981; Angelier, 1979, 1984, 1994; Petit and Laville, 1985; Means, 1987; Reches, 1987; Krantz, 1988; Lisle, 1987; Doblas, 1998). The faults in three dimension may conform to the Coloumb criterion, but due to anisotropy and inherited planes of weakness, faults may develop at angles to principal stress directions other than those predicted for isotropic media (Wojtal and Pershing, 1991). Wallace (1951) and Bott (1959) suggested that slip on pre-existing surfaces occurs parallel to the maximum resolved shear stress. After the pioneering paleostress inversion technique of Carey and Brunier (1974), a number of paleostress techniques have been developed. They have been

* Corresponding author.
E-mail addresses: nkaymakci@yahoo.com (N. Kaymakci), swhite@geo.uu.nl (S.H. White), vandijk@itc.nl (P.M. Vandijk).

0040-1951/03/$ - see front matter © 2003 Elsevier Science B.V. All rights reserved.
doi:10.1016/S0040-1951(03)00043-X

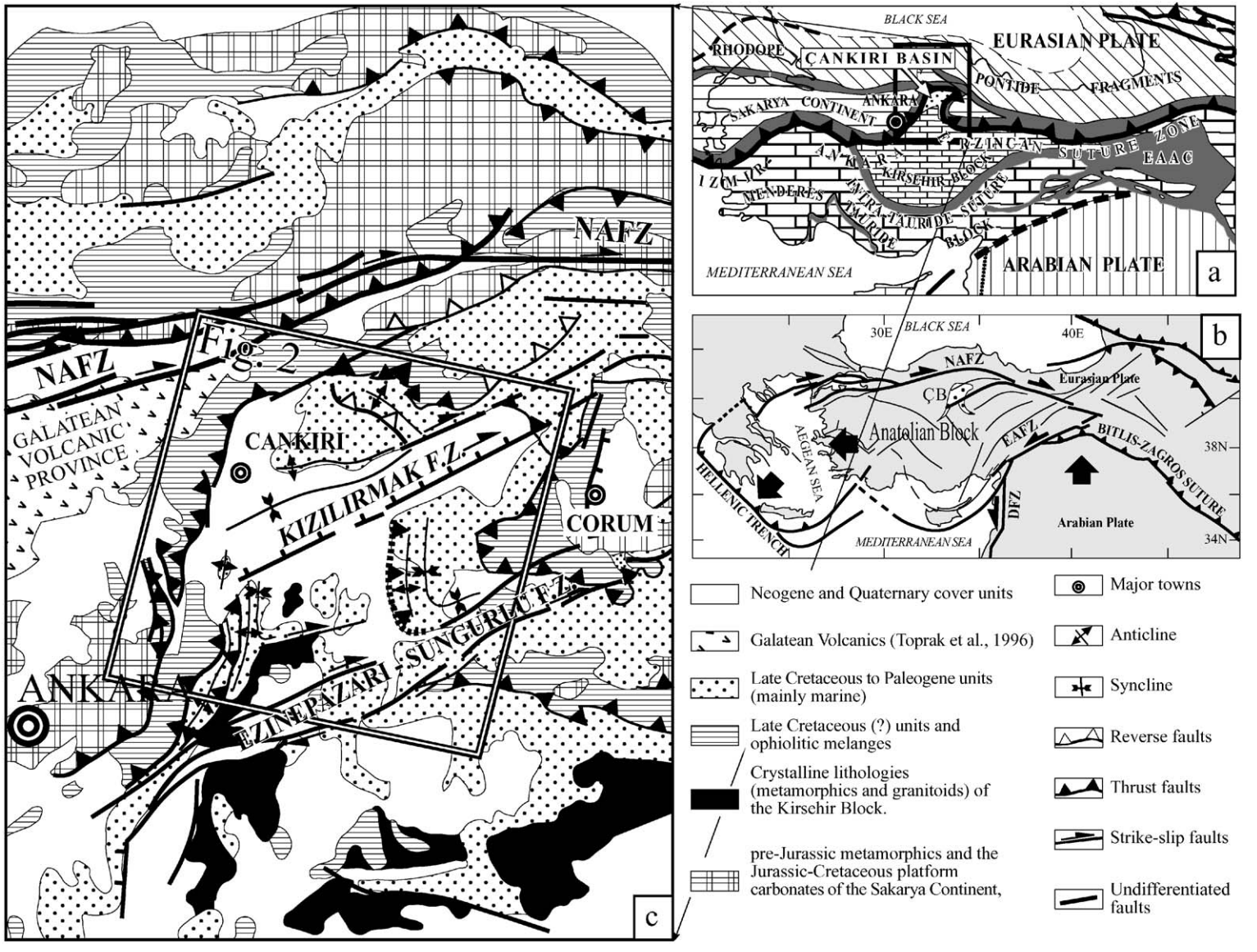
BLACK SEA
EURASIAN PLATE
RHODOPE
ÇANKIRI BASIN
PONTIDE FRAGMENTS
SAKARYA CONTINENT
ANKARA
IZMIR-ANKARA-ERZINCAN SUTURE ZONE
EAAC
MENDERES
KIRSEHIR BLOCK
INTRA-TAURIDE SUTURE
TAURIDE BLOCK
MEDITERRANEAN SEA
ARABIAN PLATE
a
30E
BLACK SEA
40E
b
NAFZ
Eurasian Plate
ÇB
Anatolian Block
EAFZ
BITLIS-ZAGROS SUTURE
38N
AEGEAN SEA
HELLENIC TRENCH
DSFZ
Arabian Plate
MEDITERRANEAN SEA
34N
NAFZ
Fig. 2
GALATEAN VOLCANIC PROVINCE
CANKIRI
KIZILIRMAK F.Z.
CORUM
SUNGURLU F.Z.
ANKARA
EZINEPAZARI
c
Neogene and Quaternary cover units
Galatean Volcanics (Toprak et al., 1996)
Late Cretaceous to Paleogene units (mainly marine)
Late Cretaceous (?) units and ophiolitic melanges
Crystalline lithologies (metamorphics and granitoids) of the Kirsehir Block.
pre-Jurassic metamorphics and the Jurassic-Cretaceous platform carbonates of the Sakarya Continent,
Major towns
Anticline
Syncline
Reverse faults
Thrust faults
Strike-slip faults
Undifferentiated faults

applied to fault slip data for a variety of tectonic context with consistent results. Thanks to this success, paleostress inversion procedures are becoming a routine analytical technique in structural geology (Pollard et al., 1993).

The purposes of this study are to apply paleostress inversion techniques to unravel the paleostress history of the southern part of the Çankırı Basin, including the Kırşehir Block (basement), and to constrain the timing of each deformation phase. We relate the results to the major structures that were active during each deformation phase. This is a complement to another study carried out in the northern part of the Çankırı Basin. Therefore, the numbering of subareas and the analytical and numerical procedures follow those outlined in detail in Kaymakci et al. (2000) and briefly described in Section 3.

2. Regional setting

The Çankırı Basin lies adjacent to the İzmir–Ankara–Erzincan Suture Zone along which the Sakarya continent (Pontides) and the Kırşehir Block (Taurides) (Fig. 1) are thought to have collided and amalgamated (Şengör and Yılmaz, 1981; Tüysüz and Dellaloğlu, 1992). Besides being affected by collisional processes, the Çankırı Basin was subjected to further deformation in the post-Late Miocene as part of the Anatolian wedge caught between the transcurrent motions on the North and East Anatolian Faults (Fig. 1). This has resulted in a number of northwards convex dextral strike-slip faults, which bifurcate from the North Anatolian Fault Zone (NAFZ) (Barka and Hancock, 1984; Şengör et al., 1985; Kaymakci and Koçyiğit, 1995). The Kızılırmak and Sungurlu Fault Zones are the two major splays of the NAFZ in this area, which partly controlled the Late Miocene evolution of the Çankırı Basin (Fig. 2).

The major structures defining the western, northern and eastern margin of the Çankırı Basin are compressional (Kaymakci, 2000; Kaymakci et al., 2000). They define a distinctive Ω-shape to the Çankırı Basin (Figs. 1 and 2). Along these faults, an ophiolitic mélange and associated Late Cretaceous volcano-sedimentary successions have been thrust over the basin fill (Akyürek et al., 1984; Dellaloğlu et al., 1992; Tüysüz and Dellaloğlu, 1992; Özçelik, 1994; Koçyiğit et al., 1995; Kaymakci et al., 1998, 2000). To the south, the granitoids of the Kırşehir Block delimit the southern margin of the basin and constitute the basement (Dellaloğlu et al., 1992; Tüysüz and Dellaloğlu, 1992; Kaymakci, 2000).

The other major structures that affected the Çankırı Basin are NE–SW trending strike-slip faults (see Figs. 1c and 2), namely, the Kızılırmak Fault Zone (KFZ), Yağbasa Faraşlı Fault Zone (YFFZ), Sivritepe Fault Zone (STFZ) and the Ezinepazarı-Sungurlu Fault Zone (ESFZ), all of which splay off the NAFZ. They cross the basin and displace the basin fill, the rim, and the basement. The south-central part of the basin is dominated by generally NNW–SSE- to NE–SW-oriented normal faults (Fig. 2). The southern area is dominated by the ESFZ, one of the major splays of the NAFZ (Fig. 1d) that partly ruptured during the Erzincan Earthquake (Mw. 7.9, 26 December 1939).

The fill of the Çankırı Basin is more than 4 km thick and accumulated during five different cycles of sedimentation (Fig. 3). The cycles are discussed in detail in Kaymakci (2000) and only a summary is given here. The oldest cycle comprises the Late Cretaceous volcanoclastics and regressive shallow marine units, and the Paleocene mixed environment red clastics and carbonates (Özçelik, 1994; Kaymakci, 2000). The second cycle is a Paleocene to Oligocene regressive flysch to molasse sequence overlain by a widespread thin (< 100 m) nummulitic limestone, Middle Eocene in age, that passes into very

Fig. 1. (a) Inset map showing the geological outline of the Eastern Mediterranean area (modified after Görür et al., 1984; Şengör et al., 1984). EAAC: East Anatolian Accretionary Complex. (b) Active tectonic outline of Turkey and surrounding regions (modified after Barka and Hancock, 1984; Şengör et al., 1985; Koçyiğit, 1989; Özçelik, 1994; Kaymakci and Koçyiğit, 1995). ÇB: Çankırı Basin, DFZ: Dead Sea Fault Zone, EAFZ: East Anatolian Fault Zone, NAFZ: North Anatolian Fault Zone. Large black arrows are the movement directions of Arabian plate and Aegean–Anatolian Block. (c) Detailed tectono-stratigraphical map of the central Anatolia. Box shows the location of the study area. Concentric circles are major towns.

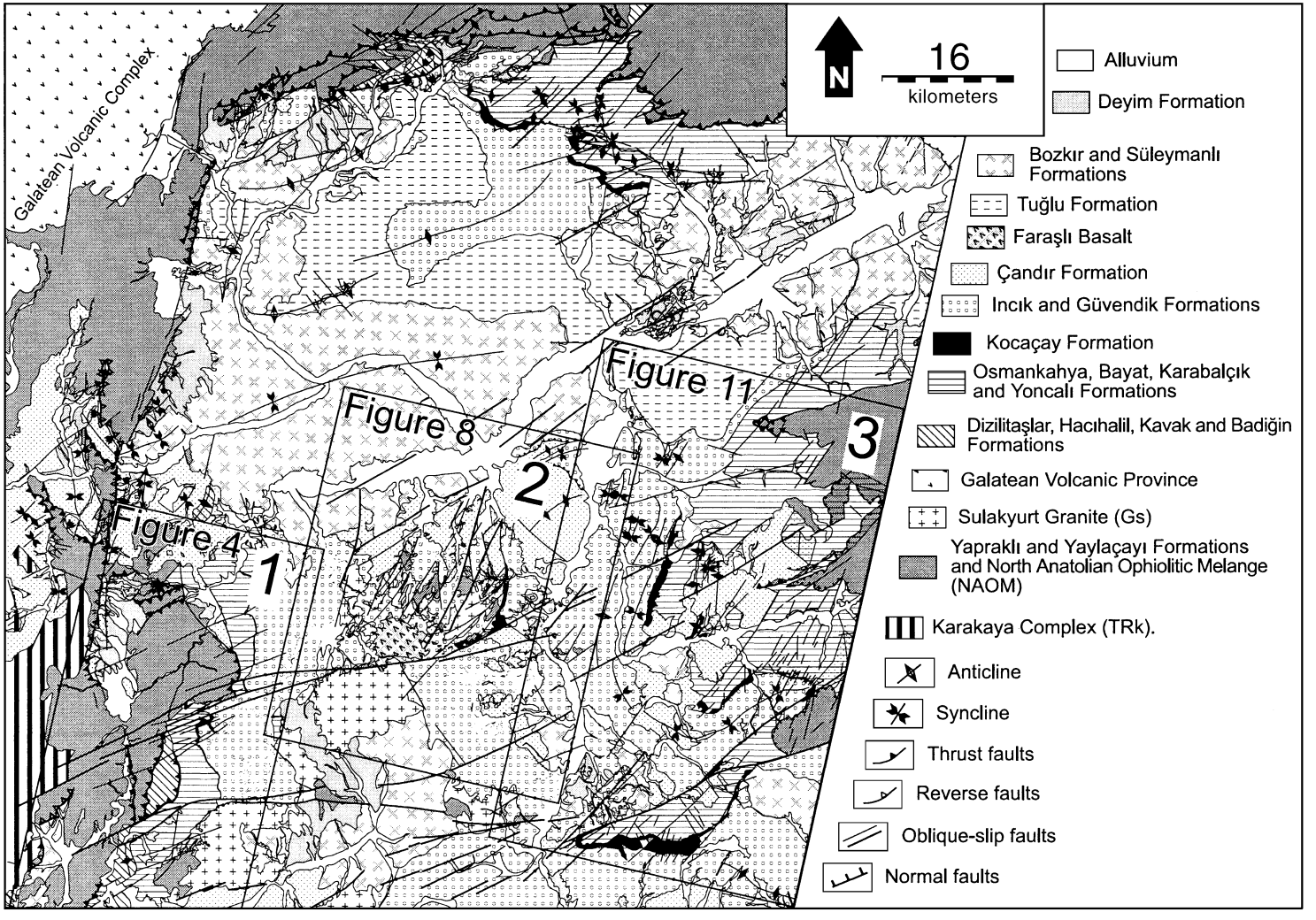

Fig. 2. Geological map of the Çankırı Basin. The numbers and the boxes indicate the locations of the subareas.

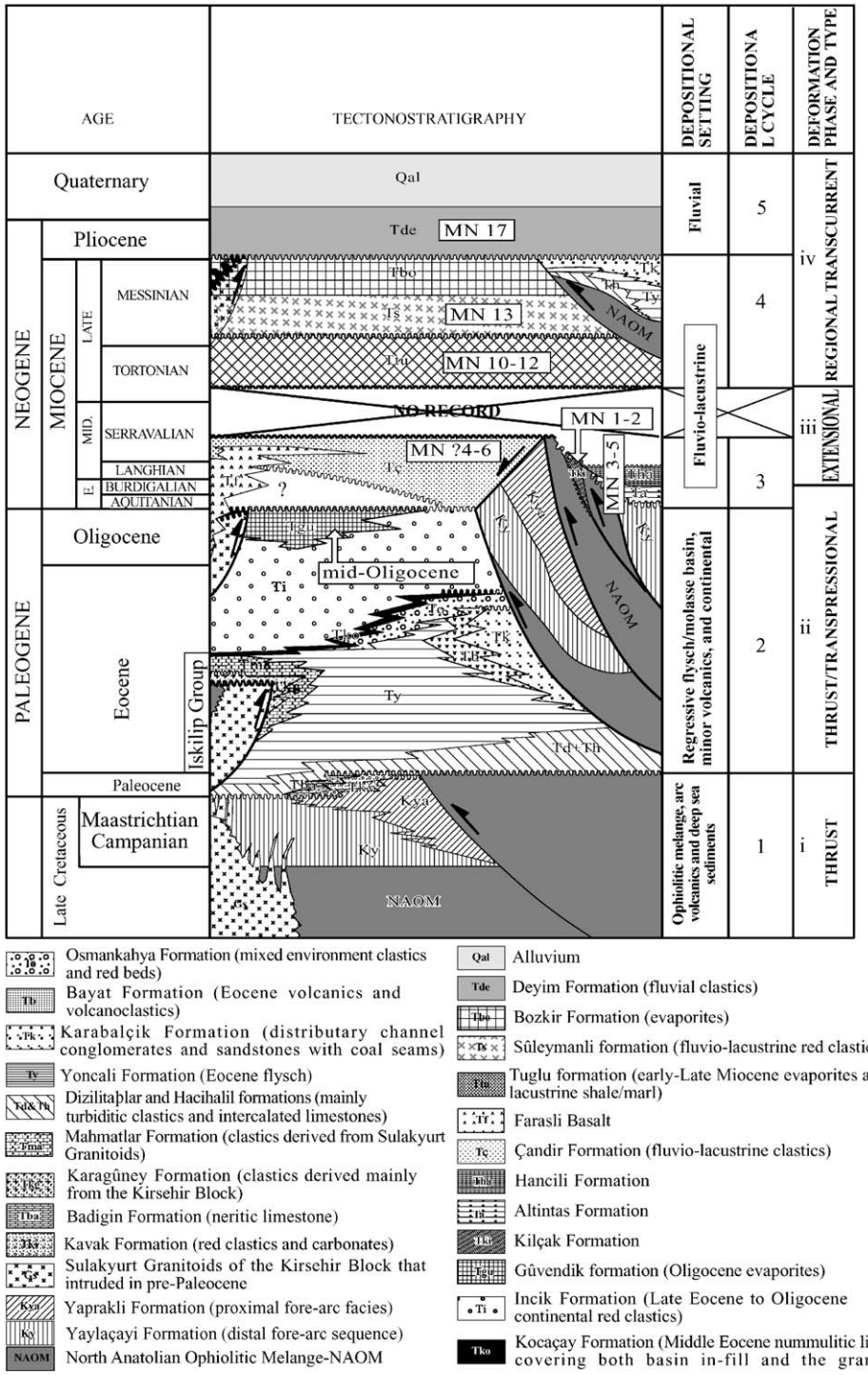

Fig. 3. Generalized tectono-stratigraphic column for the units exposed in and around the Çankırı Basin. MN zones are after Kaymakci et al. (2001b).

thick (up to 2000 m) Late Eocene to Oligocene continental red clastics intercalated with and overlain by the Oligocene evaporites. The third cycle is represented by fluvio-lacustrine clastics deposited in the Early to Middle Miocene. The fourth cycle is represented by the units that were deposited in Late Miocene fluvio-lacustrine conditions. They frequently alternate with evaporites. The Plio-Quaternary alluvial fan deposits and recent alluvium locally overlie all of these units (Fig. 3) and form the fifth cycle.

3. Methodology

In the southern part of the Çankiri Basin, more than 280 fault-slip data from 32 sites have been collected. The relative ordering of fault motions and related deformation was established from overprinting and cross-cutting relationships. The age constraints were applied through the careful documentation and analysis of the fault structures in each of the stratigraphical horizon. To avoid problems due to relative block and fault plane interactions (see Pollard et al., 1993; Twiss and Unruh, 1998) and to keep structural homogeneity, sampling sites were kept to less than 50 m diameter (Hancock, 1985). Areas larger than this were subdivided into subsites and analyzed independently. In addition, the faults with less than 1-m displacement were used in the analysis because they should accommodate small strain associated with parallel principal strain and stress axes (Hardcastle, 1989).

Relative age of each movement phase was determined independently for each fault and carefully correlated with data from other subareas to form a regional subset, which is then processed following the algorithm proposed in Kaymakci et al. (2000). During the analyses, the data from each site were carefully examined and correlated to the site within a subarea. The slip data, which have the same order of occurrence, could be grouped together for preliminary stress inversion processing (Kaymakci et al., 2000). For computational processing of the data, Angelier's method was used (see Angelier, 1984, 1994, for an overview of the stress inversion procedure).

After preliminary processing, faults having more than 15° misfit angle were considered spurious, separated from the data set and treated separately. After removal of spurious data, the stress tensor was re-computed and re-analyzed using the software developed by Hardcastle and Hills (1991) for the automatic separation of stress tensors associated with the different deformation phases as indicated from the field observations. Concordant data were then taken as indicating that the computed stress tensor is likely correct. The initial spurious data were re-computed by the Hardcastle and Hills (1991) method and if again spurious they were not used in the final construction of the stress tensors. If concordant (both in direct inversion method and automated separation process) they were included and re-analyzed. It should be kept in mind that automatic separation was used only to verify the results obtained from Angelier's method. By this way results were cross-checked.

In order to determine the mean stress tensor configuration for a given movement phase in each subarea, all the data from each site and each phase were grouped and the above procedure repeated. After the mean stress orientations were determined, all of the raw data was re-processed and the results were compared with those obtained using the direct inversion method. Because the minimum number of slickenline data required to construct a stress tensor is 4 in the direct inversion method (Angelier, 1979), the data of sites containing less than this number was used only in the construction of mean stress tensor for the subarea within which it was located.

After the stress tensors for each set at each site had been determined, they were correlated between sites. By combining the stratigraphic information and the relative order of the different sets, the stress tensors were arranged into ordered deformation phases.

In both the direct inversion and the Hardcastle–Hills methods, 15° was chosen as the maximum angular deviation acceptable for the computation of a given stress tensor. Faults with greater angular deviations, after re-groupings and re-calculations, were considered to be spurious and deleted. Ten percent (10%) of the whole data set falls into this category.

4. Field observations and results

The southern part of the Çankırı Basin is subdivided into three subareas (Fig. 2) based on marked differences in the underlying lithologies, and type and trends of the structures.

4.1. Subarea 1

Subarea 1 lies in the southwestern part of the Çankırı Basin where the basement and the rim come closer to each other than at any other part of the basin (Fig. 4). They are separated from each other by the Late Cretaceous to Paleocene and Late Paleocene to Middle Eocene units. The main structures in the subarea are faults and folds (Fig. 4).

4.1.1. Faults

The main faults observed in this area are the Bedesten Faults (BTF-1, BTF-2, and BTF-3), Malıboğazı Trust Faults (MTF), Kazmaca–Hamzalı Reverse Fault (KHRF), Sivritepe Fault (STF), Kılçak Thrust Fault (KLTF), Kayadibi Fault (KDF), Babas–Ekincibayırı Fault (BETF) and Hıdırşeyh Thrust Fault (HITF) (Fig. 4). Most of these faults delimit the western rim of the basin and are dextrally displaced by the substrands of

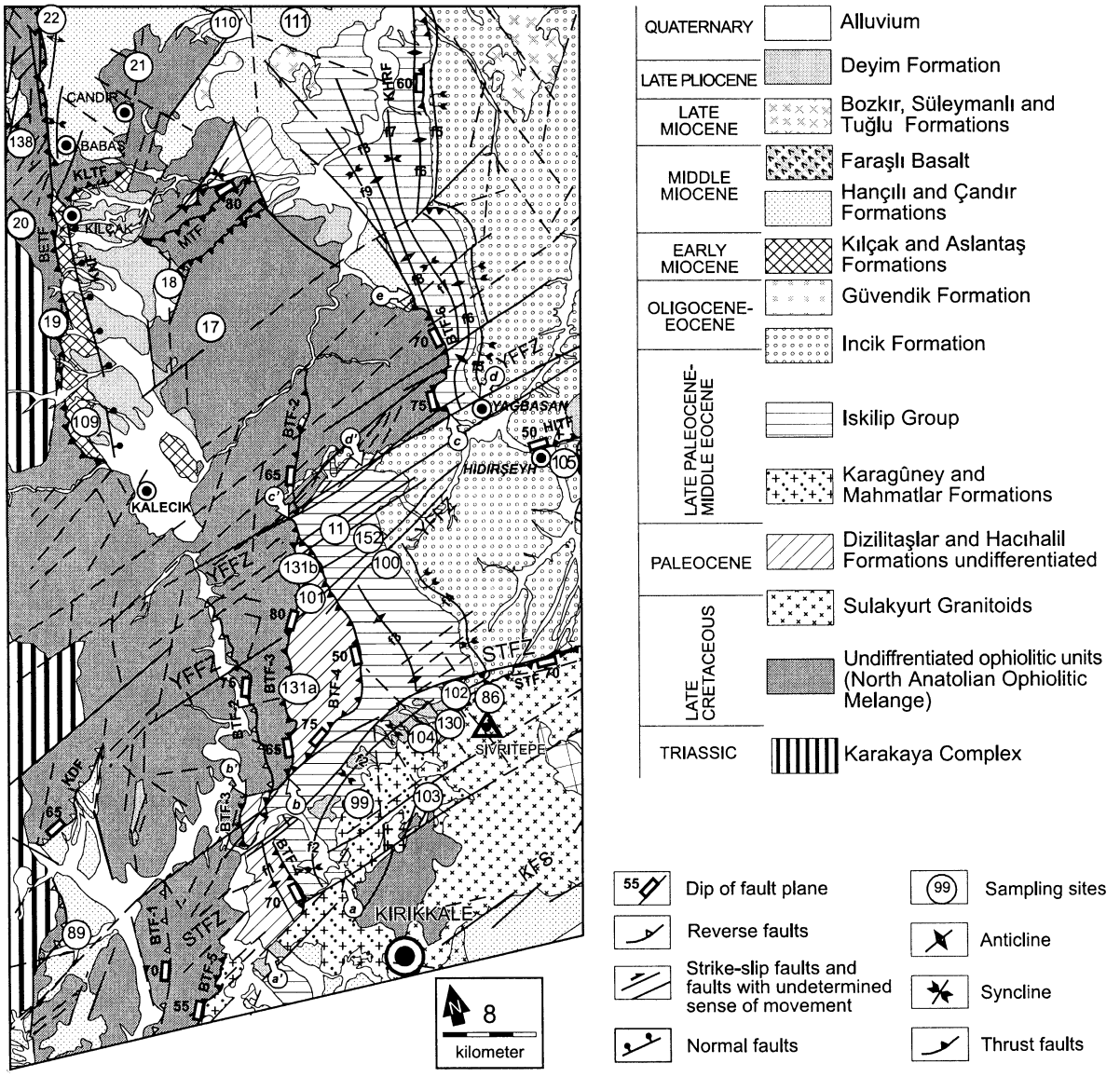

Fig. 4. Geological map and sample locations for subarea 1 (see Fig. 3 for the ages of the stratigraphical units).

the Yağbasan–Faraşlı (YFFZ) and Sivritepe Fault Zones (STFZ). The structural characteristics and possible age ranges of these faults are outlined in Fig. 5.

Along the faults BTF-1 and -2, various constituent units of the North Anatolian Ophiolitic Mélange (NAOM) are intensely deformed and sheared. No reliable slickenlines were observed. Along the fault BTF-3, the NAOM tectonically overlies the Late Cretaceous to Paleocene Dizilitaşlar Formation (Fig. 4). The Dizilitaşlar Formation, in turn, has

FAULTS

Faults	hanging wall Formations	foot wall Formations	covering or youngest displaced Formation	dip range and direction of the fault plane	Possible age range of the fault activity	Deform. style	AGE
STF	Sulakyur Granite	Ty, Tk, To Incik (Ti)	Deyim (Late Pliocene-Quat)	70˚S	Late Miocene to Recent	TRANS-CURRENT	post-Middle Miocene
KDF	NAOM	Çandir	Çandir (Middle Miocene)	70˚-80˚W	post-Middle Miocene		
BETF	NAOM, Ky, Kya	Çandir	Süleymanli (Late Miocene)	60˚-80˚W	post-Middle Miocene pre-Late Miocene		
BTF-1 BTF-2	NAOM, Yalaçayi (Ky), Yaprakli (Kya)	NAOM, Ky, Kya	NAOM (Late Cretaceous)	65˚-75˚W	Late Cretaceous to Recent	TRANSPRESSION	PRE-MIDDLE MIOCENE (?)
BTF-3	NAOM, Ky, Kya	Dizilitaşlar (Td)	Dizilitaşlar (Paleocene)	65˚-80˚W	post-Paleocene		
BTF-4	Td	Yoncali (Ty) Karabalçik (Tk)	Karabalçik (Middle Eocene)	50˚-70˚W	Early to Middle Eocene to Recent		
BTF-5	Td	Ty, Tk	Mahmatlar (Eocene)	55˚W			
BTF-6	NAOM, Ky, Kya	Tk	Çandir (Tç) (Middle Miocene)	70˚-75˚W	Middle Eocene, pre-Middle Miocene		
MTF	NAOM	Kya	Deyim (Tde) (Late Pliocene-Quat.)	20˚-45˚S	post-Late Cretaceous pre-Late Pliocene		
KHRF	Kocaçay (Tko), TK	Incik	Çandir (Middle Miocene)	60˚-90˚E	Middle Eocene to pre-Middle Miocene		
KLTF	NAOM, Ky	Kilçak	Deyim (Late Pliocene-Quat.)	35˚-70˚N	post-Early Miocene pre-Late Pliocene		

Faults	Displaced youngest formations	Max. offset	Along strike changes in def. style	dip range and direction of the fault plane	Possible age range of the fault activity	Deform. style	AGE
YFFZ	Bozkir and Süleymanli	c-c'=13km d-d'=9 km	Transpression to transtension	70˚N to 70˚S	syn- to post-Late Miocene	Transpression/ Transtension	post-Middle Miocene
STFZ	Süleymanli	a-a'=7km b-b'=3km	transpression to transtension	70˚N to 65˚S	syn- to post-Late Miocene		
KFS	Süleymanli	?	transtension	60˚N to 90˚S	syn- to post-Late Miocene		

FOLDS

folds	youngest folded unit	Covering unit	dip range and direction of the axial plane	possible compression direction	Age range
f1	Td		70˚-90˚N	E-W	post-Paleocene
f2	Ty		60˚-90˚N	NW-SE	post-Mid. Eocene
f3	Ty, Tk		70˚-90˚N	E-W	post-Mid. Eocene
f4, f5	Ti		35˚-60˚N	E-W	syn- to post-Mid. Eocene
F6-f9	Tk	Tç	50˚-90˚N	E-W	syn- to post-Mid. Eocene to pre-Middle Miocene

Fig. 5. Figure illustrating the structural and kinematic characteristics, possible age ranges of the faults and the folds developed in subarea 1. BTF: Bedesten Faults, MTF: Malıboğazı Fault, KHRF: Kazmaca–Hamzalı Fault, KLTF: Kılçak Thrust Fault, STF: Sivritepe Fault, KDF: Kayadibi Fault, BETF: Babas–Termeyenice Fault, YFFZ: Yağbasan–Faraşlı Fault Zone, STFZ: Sivritepe Fault Zone, KFS: Kırıkkale Fault set.

been thrusted over the Early to Middle Eocene Karabalçık and Yoncalı Formations along the fault BTF-4. Along the fault BTF-5 the NAOM tectonically overlies the Early to Middle Eocene Mahmatlar Formation in the southwesternmost part of the basin. This relationship is important for determining the amount of E–W tectonic transport of the rim. The Mahmatlar Formation is derived mainly from the Kırşehir Block and lies adjacent to it (Kaymakci, 2000). It is separated from the rim of the Çankırı Basin by the Late Cretaceous to Paleocene Dizilitaşlar Formation and from the Early to Middle Eocene units (Yoncalı and Karabalçık Formations). Therefore, the cumulative vertical offset of this fault is larger than the total thickness of these units, which is more than 2 km. In the north, along the fault BTF-6, the NAOM is thrusted over the Early to Middle Eocene Karabalçık Formation. It is unconformably overlain by the latest-Early Miocene to Middle Miocene (MN ?4–6) Çandır Formation where it is displaced by a NW–SE trending normal fault (location e in Fig. 4) indicating post-Middle Eocene and pre-latest-Early Miocene to Middle Miocene activity of this thrust fault.

The Kılçak Thrust Fault (KLTF) is the youngest well-constrained thrust fault observed in the Çankırı Basin. Along the KLTF, the NAOM and the Yaylaçayý Formation have been thrusted over the Aquitanian (MN 1–2) Kılçak Formation.

The Yağbasan–Faraşlı and Sivritepe Fault Zones have displaced the rim, the basin fill, including the Late Miocene units, and the basement (Fig. 4) indicating the syn- to post-Late Miocene activity.

4.1.2. Folds

The folds (f1–f9) developed in this subarea are oriented mainly in a N–S to NNW–SSE direction except f2, which has a curved trace and becomes parallel to the SFZ in the north (Fig. 4). The folds f1 and f3 trend parallel to the fault BTF-4, which leads for a common tectonic origin. The folds (f5–9) in the north of the YFFZ are subparallel to the BTF-6 and trend NNW–SSE to N–S. In addition, the folds f8–f9 are overridden by the BTF-6 indicating their sequential development. The folds f4 and f55 are overturned synclines developed within the Incik Formation and associated with progressive unconformities within the Incik Formation. This relation was interpreted as being due to the coupling of thrusting and deposition of the Incik Formation in the post-Middle Eocene to pre-Oligocene (Kaymakci, 2000). The characteristics of these folds are summarized in Fig. 5.

4.1.3. Paleostress inversion

In order to understand the kinematic history of this subarea, 91 out of 105 fault slip data have been analyzed from 17 sites (Fig. 6). The remaining 14 data were spurious. Therefore, they were not used in the construction of stress tensors. With the exception of sites 109 and 89 where the data was collected from Aquitanian (MN 1–2) Kılçak Formation and the NAOM, respectively, all the other data were collected from Paleocene to Eocene units. The details of the data from each site are given in Table 1.

At seven sites, two different sets of overprinting slickenlines and slickenfibres developed in the dilatational jogs and three different fault movements were observed in the field (Table 1). In ordering of movement sets and deformation phases, the procedure discussed in Kaymakci et al. (2000) was followed as mentioned before.

Phase 1: This phase is recognized at only six sites (Fig. 6a and Table 2). The orientation of the horizontal principal stress is relatively consistent between sites and it is oriented ENE–WSW to NNE–SSW. Except for sites 109 and 131-2 in which σ_3 is vertical, in all other sites σ_2 and σ_3 are oblique (see Table 2).

The orientations of the subarea based mean regional stresses are as follows $\sigma_1 = 023°\text{N}/01°$, $\sigma_2 = 116°\text{N}/64°$, $\sigma_3 = 293°\text{N}/26$ (Fig. 7 and Table 2). The youngest unit which has been deformed in this phase is the MN-1 Kılçak Formation. Therefore, deformation phase 1 postdates the deposition of the Kılçak Formation in the Aquitanian (MN 1–2 in MN zones, Fig. 3). The approximately subvertical orientation of σ_2 and oblique orientation of σ_3 indicate transcurrent deformation in the deformation phase 1.

Phase 2: This phase was recognized at two sites (Fig. 6). In both sites σ_1 is subvertical and σ_3 is subhorizontal and σ_2 is subhorizontal (Fig. 6 and Table 2). The orientations of the mean regional stresses are as follows: $\sigma_1 = 303°\text{N}/67°$, $\sigma_2 = 075°\text{N}/16°$, $\sigma_3 = 170°\text{N}/17$ (Fig. 7 and Table 2). The subvertical orientation of σ_1 and approximately subhorizontal orientation of the other principal stress indicate a dominantly extensional deformation.

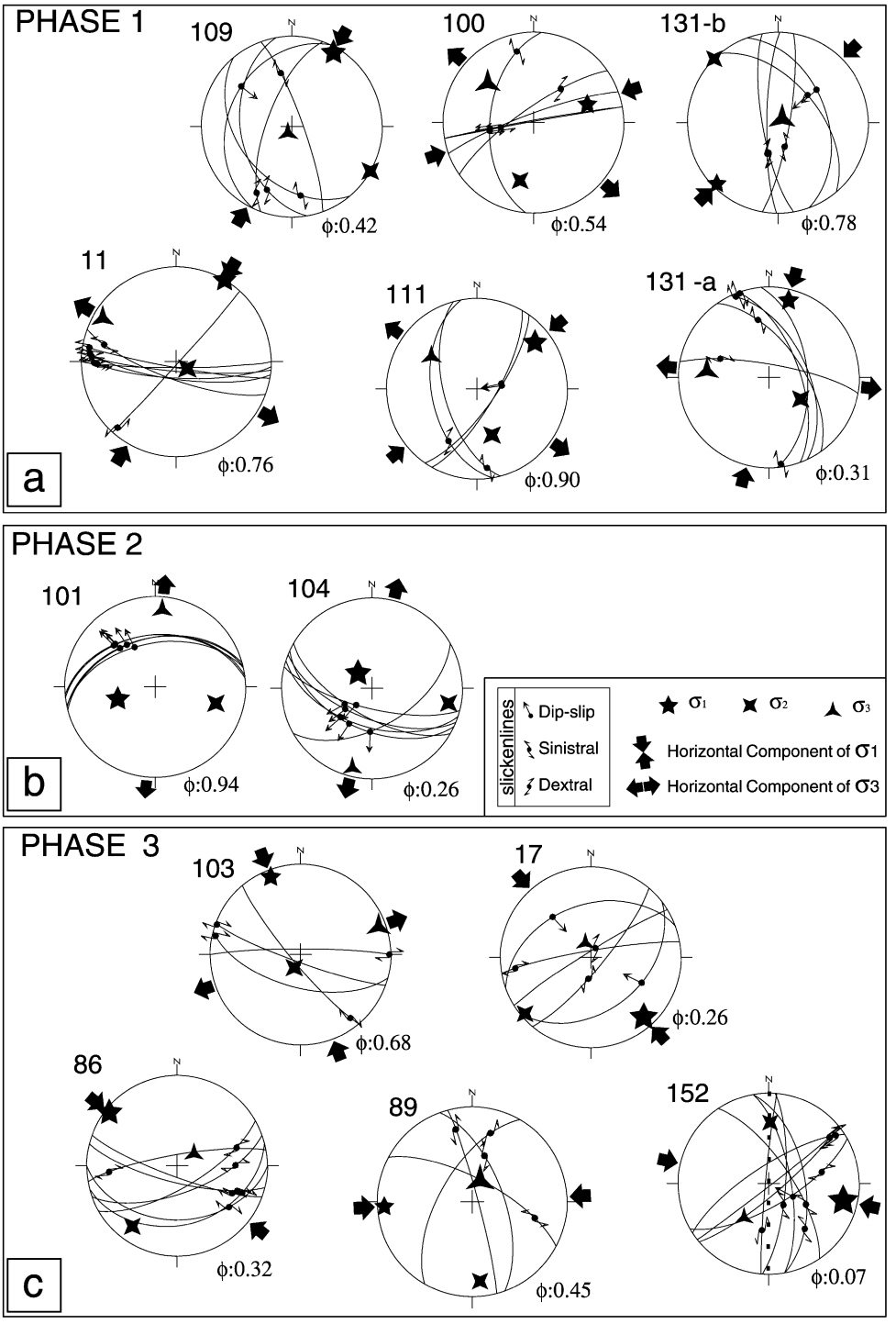

Fig. 6. Plots of faults planes, slickenlines, and stress orientations for each site in subarea 1 (lower hemisphere, equal area projection).

Table 1
Kinematic field characteristics of the faults and their hosting units for each site in each subarea

	Site	Type of indicators	Associated fibres	Number of cross-cutting	Vein	Host unit	Number of phases
Subarea 1	11	Slickenlines/fibre	Calcite	2	–	Karabalçık	2
	17	Slickenlines	–	2	–	İncik	2
	86	Slickenlines	–	–	–	Mahmatlar	2
	89	Slickenlines	–	2	–	NAOM	2
	99	Slickenlines	–	–	–	Dizilitaşlar	1
	100	Slickenlines/fibre	Calcite	2	+	Kocaçay	2
	101	Slickenlines/fibre	Calcite	2	+	Kocaçay	2
	102	Slickenlines	–	–	–	Mahmatlar	2
	103	Slickenlines	–	–	–	Mahmatlar	1
	104	Slickenlines	–	–	–	Mahmatlar	1
	105	Slickenlines	–	–	–	Mahmatlar	1
	109	Slickenlines/hyd.P.S.	–	2	+	Kılçak	2
	111	Slickenlines/hyd.P.S.	–	2		Hacıhalil	2
	130	Slickenlines	–	–	–	Hacıhalil	1
	131-a	Slickenlines/fibre	Calcite	2	+	Hacıhalil	2
	131-b	Slickenlines/fibre	Calcite	2	+	Karabalçık	2
	152	Slickenlines/fibre	Calcite	2	+	Karabalçık	2
Subarea 2	90	Slickenlines	–	1	–	Sulakyurt Granite	1
	92	Slickenlines	–	1	–	Sulakyurt Granite	1
	94	Slickenlines		1		İncik	1
	95	Slickenlines		1	–	İncik	1
	98	Slickenlines		1		İncik	1
	146	Slickenlines/fibre	Calcite	2	+	Çandır	2
	148	Slickenlines/fibre	Calcite	2	+	İncik	2
Subarea 3	76	Slickenlines/fibre	Calcite	3	+	Yoncalı	3
	120	Slickenlines/fibre	Calcite	3	+	Yoncalı	3
	121	Slickenlines/fibre	Calcite	3	+	İncik	3
	122-A	Slickenlines/fibre	Calcite	3	+	Yoncalı	3
	122-B	Slickenlines/fibre	Calcite	3	+	Yoncalı	3
	124	Slickenlines/fibre	Calcite	3	+	Yoncalı	3
	125	Slickenlines/fibre	Calcite	3	+	Yoncalı	3
	132	Slickenlines/hydroplastic slickensides	Calcite	2	+	Osmankahya	2
	148-A	Slickenlines/fibre	Calcite	2	+	Yoncalı	2
	148-B	Slickenlines/fibre	Calcite	2	+	Çandır	2
	149	Slickenlines	–	2	–	Tuğlu	2
	150	Slickenlines	–	2	–	Tuğlu	2
	151	Slickenlines/fibre	Calcite	2	+	Candır	2

Slickenlines/fibre: polished surfaces and growth fibres. Number of cross-cutting: number of cross-cutting and/or overprinting sets of kinematic indicators of any type. Number of phases corresponds to the number of phases of deformation encountered in each site. They do not necessarily correspond to the order of phases. NAOM: North Anatolian Ophiolitic Mélange. + Present, – absent.

Phase 3: Only five sites had sufficient data for the construction of stress tensors (Fig. 6 and Table 2). The horizontal component of the σ_1 ranges from E–W to NNW–SSE. Except for site-103 where σ_2 is subvertical, in the other sites σ_3 is subvertical. The mean stresses for the subarea are $\sigma_1 = 113°\text{N}/13°$, $\sigma_2 = 017°\text{N}/25°$, and $\sigma_3 = 228°\text{N}/62°$. Having the regional σ_3 subvertical, σ_2 subhorizontal and σ_1 horizontal suggests compressional deformation in this subarea.

4.2. Subarea 2

4.2.1. Faults

The main structures shaping subarea 2 are the Yağbasan–Faraşlı Fault Zone (YFFZ), generally N–S- to

Table 2
Orientations of principal stresses and stress ratios for each site in each subarea

		Site	σ_1	σ_2	σ_3	ϕ	Number of faults
Subarea 1	Phase 1	11	031/00	121/79	301/11	0.51	7
		100	071/37	193/35	311/34	0.72	5
		109	029/07	119/00	211/84	0.38	5
		111	051/19	162/46	305/38	0.40	4
		131-a	014/13	124/55	276/32	0.64	5
		131-b	225/05	315/00	046/85	0.78	5
		Regional	023/01	116/64	113/13	0.37	35
	Phase 2	101	252/54	105/31	005/16	0.46	5
		104	318/71	101/15	194/11	0.32	6
		Regional	303/67	075/16	017/25	0.32	30
	Phase 3	17	138/13	229/05	339/76	0.24	5
		86	308/05	216/18	054/71	0.32	7
		89	267/08	174/17	021/71	0.84	4
		103	339/09	206/77	70/09	0.66	4
		152	103/17	001/33	216/52	0.15	9
		Regional	150/24	300/64	228/62	0.26	23
Subarea 2	Phase 1	95	016/29	161/56	277/16	0.46	5
		Regional	056/10	255/80	147/03	0.60	13
	Phase 2	92	167/45	048/27	298/33	0.46	6
		94	206/73	033/17	302/02	0.13	8
		98	197/55	002/34	097/07	0.53	5
		Regional	180/59	357/31	088/01	0.45	11
	Phase 3	90	130/46	317/44	224/03	0.54	5
		146	137/38	290/49	036/14	0.93	4
		Regional	123/39	308/51	041/02	0.67	9
Subarea 3	Phase 1	76	013/18	253/57	112/27	0.26	5
		120	195/04	356/86	105/01	0.51	6
		121-a	172/14	333/75	081/05	0.49	10
		122-b	174/17	335/72	081/06	0.43	6
		125	205/02	296/33	112/57	0.39	5
		150	042/02	137/69	311/21	0.26	12
		Regional	199/03	306/80	109/10	0.34	36
	Phase 2	120	324/62	118/26	213/11	0.99	7
		121-a	086/86	287/03	197/01	0.27	5
		132	355/73	107/06	199/15	0.32	5
		Regional	080/77	299/10	207/08	0.64	20
	Phase 3	76	107/14	303/75	198/04	0.25	10
		124	111/23	294/67	201/01	0.72	7
		148-b	103/27	221/42	351/36	0.25	4
		149	142/29	349/58	239/12	0.38	11
		151	087/27	266/63	356/00	0.55	13
		Regional	100/23	285/67	191/02	0.38	64

NE–SW-oriented normal faults with sinistral components, the Halaçlı Fault (HTF), and the Kızılırmak Fault Zone (KFZ) (Fig. 8).

The YFFZ extends from subarea 1 where it is a strike-slip fault with a component of normal sense of movement as indicated by the slickenlines and slickenfibres developed in dilational jogs.

The Halaçlı Thrust Fault (HTF) is observed in the NE corner of the subarea. Along the HTF, the Oligocene Gűvendik Formation tectonically overlies the latest-Early Miocene to Middle Miocene (MN ?4–6) Çandır Formation. The HTF is displaced more than 7 km dextrally by one of the faults within the Kızılırmak Fault Zone (Fig. 8). Based on this information it can be

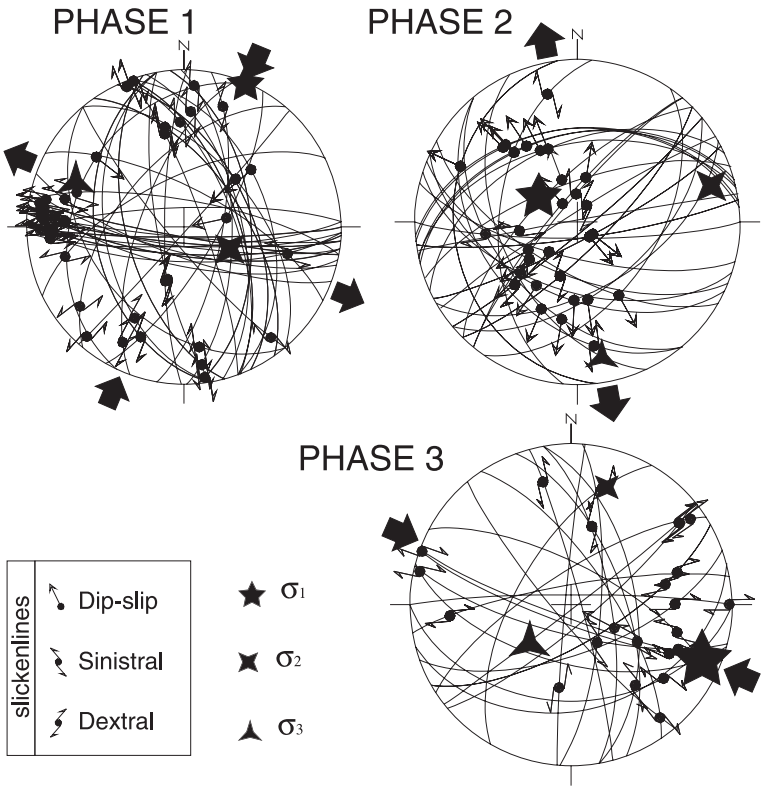

Fig. 7. Plots of fault planes, slickenlines and stress orientations for the whole data, in subarea 1, for each deformation phase.

concluded that the HTF postdates the deposition of the Çandır Formation in latest-Early Miocene to Middle Miocene and predates the Kızılırmak Fault Zone.

Along the N–S- and NE–SW-oriented faults (Fig. 8), to the north of the YFFZ, the Sulakyurt Granitoids, Kocaçay, Incik, and Çandır Formations are displaced dominantly in normal sense with slight lateral components. In the north, these faults are covered by the Messinian (MN-13) Sűleymanlı Formation and further in the north some of these faults are partly delimited by the Kızılırmak Fault Zone. These faults were normal faults during the deposition of the Çandır Formation in the latest-Early Miocene to Middle Miocene (MN ?4–6) period (Kaymakci et al., 2000). They were later inverted into reverse faults in post-Messinian times.

The Kızılırmak Fault Zone, in this part of the Çankırı Basin, is characterized by NE–SW-oriented strike-slip faults with normal component (Kaymakci et al., 2001a) that have displaced the HTF, and the Messinian (MN-13) Sűleymanlı and Bozkır Formations, indicating post-Messinian activity of the Fault.

4.2.2. Paleostress inversion

From 10 sites, 43 fault slip data have been collected. In five of the sites, overprinting slickenlines were observed indicating two different episodes of fault movements. The number of faults used in the paleostress computations varies between four and eight, which decreases the reliability of the results for each site. However, subarea-based tensors were reconstructed using all of the data including the sites, which do not have enough slip data for site-based analysis as well. Ordering of the deformation phases was based on overprinting relationships, the automated separation procedure and correlation with the other subareas. The details of the sites are given in Table 1.

Phase 1: Only one site had enough slip data for the inversion procedure. The orientation of the site-based

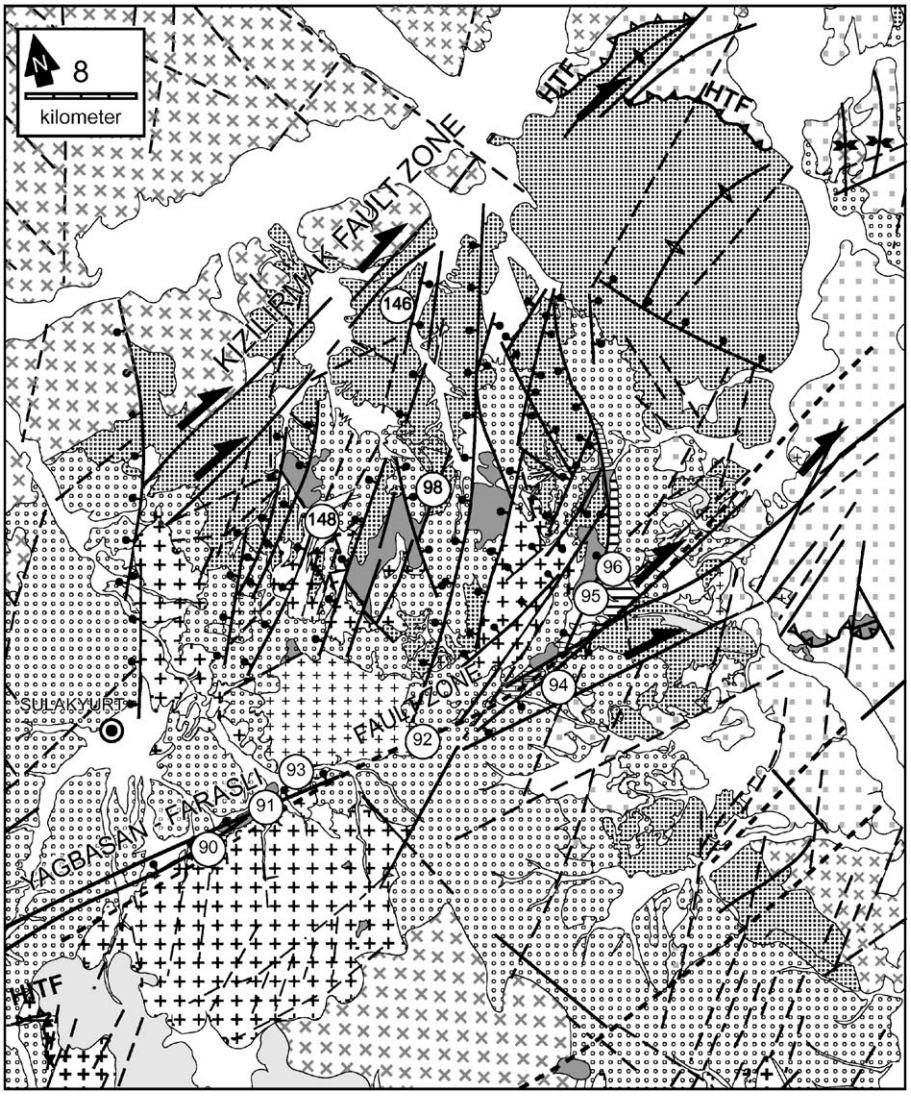

Fig. 8. Geological and sample location (site) map for subarea 2 (same legend as Fig. 4). HTF: Halaçlı Thrust Fault.

tensors is given in Table 2 and Fig. 9. The orientations of the subarea-based regional stresses are as follows: $\sigma_1 = 056°\text{N}/10°$, $\sigma_2 = 255°\text{N}/80°$, and $\sigma_3 = 147°\text{N}/03°$ (Fig. 10 and Table 2), indicating strike-slip regime in this part of the basin during deformation phase 1.

Phase 2: This deformation phase was recognized in only three sites (Fig. 9). In each site, σ_3 is subhorizontal and σ_1 is subvertical. The orientations of the principal stresses are consistent and are as follows: $\sigma_1 = 180°\text{N}/59°$, $\sigma_2 = 357°\text{N}/31°$, $\sigma_3 = 088°\text{N}/01$ (Fig. 10 and Table 2) and indicate oblique-extensional deformation in the area during this phase.

Phase 3: Two sites had enough slip data for the construction of site-based stress tensors. The orientations of the principal stresses are given in Fig. 9 and Table 2. All of the faults used in the construction of the regional stress have dextral strike-slip character which decreases the precision of the results. They may only indicate the average orientations of the principal stresses. The orientations of the regional principal stresses are as follows: σ_1 is subhorizontal and trend-

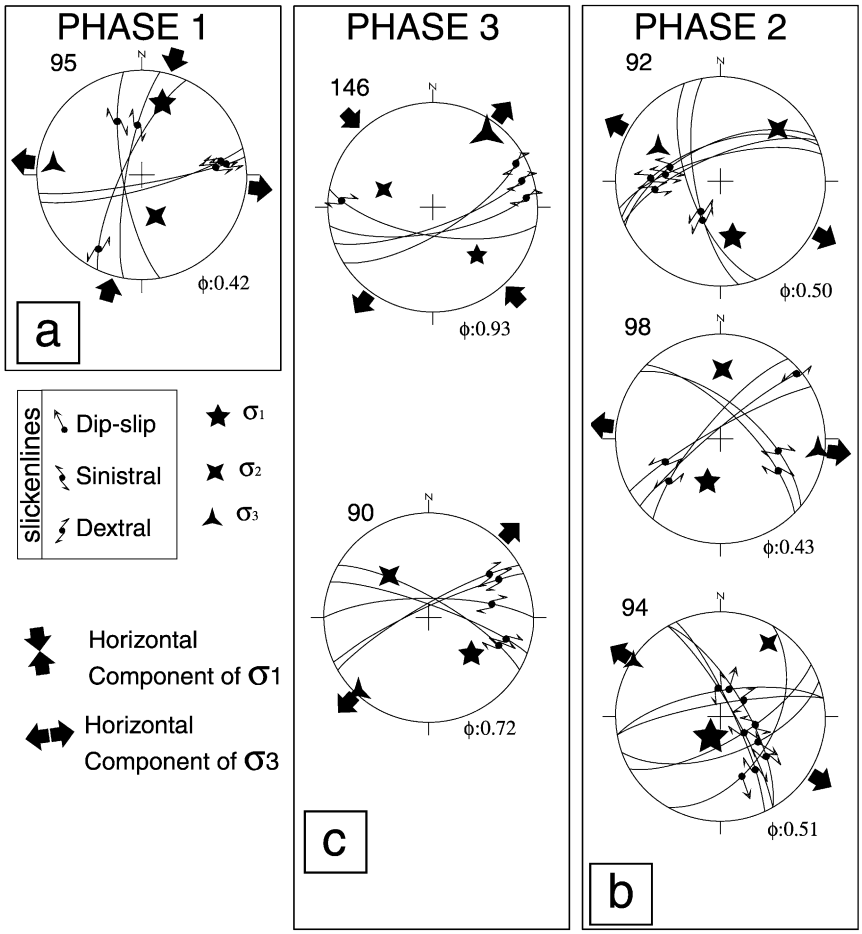

Fig. 9. Plots of faults planes, slickenlines, and stress orientations for each site in subarea 2 (lower hemisphere, equal area projection).

ing NW–SE (123°N/39°), σ_2 is subvertical (308°N/51°), and σ_3 is horizontal and trending NE–SW (041°N/02°) (Fig. 6d and Table 2). Subvertical σ_2 and subhorizontal σ_1 and horizontal σ_3 suggest transtension in this part of the basin in deformation phase 3.

4.3. Subarea 3

4.3.1. Faults

The main structures in subarea 7 are the Uğurludağ Thrust faults (UTF 1–4), the Tuğcu Faults (TGF 1 and 2), the Sağpazar Reverse Fault (SRF), the Karaçay Reverse Fault (KARF), the Gűvendik Thrust Fault (GTF), the Sungurlu Fault Zone and its main strand (MSFZ), the Gűvendik Folds (GF) and the Sağpazar Anticline (SA) (Fig. 11).

The basic characteristics of SRF, KARF, GTF, and MSFZ and their tectonic implications are summarized in Fig. 12.

The Uğurludağ Thrust Faults (UTF 1, UTF 2, UTF 3, and UTF 4) are the most prominent structures in this subarea. Along the UTFs, the NAOM and associated Late Cretaceous units are thrusted over most of the Early to Middle Eocene units (the Yoncalı, Karabalçık, Bayat and Osmankahya Formations), indicating post-Middle Eocene activity (Figs. 11 and 12). The UTFs are displaced dextrally by a number of NE–SW-trending strike-slip faults, and therefore, the primary relation between UTF 2 and UTF 3 is obliterated. Among these, UTF 1 is a reverse fault with a dextral strike-slip component. The kinematic characteristics of the other UTFs,

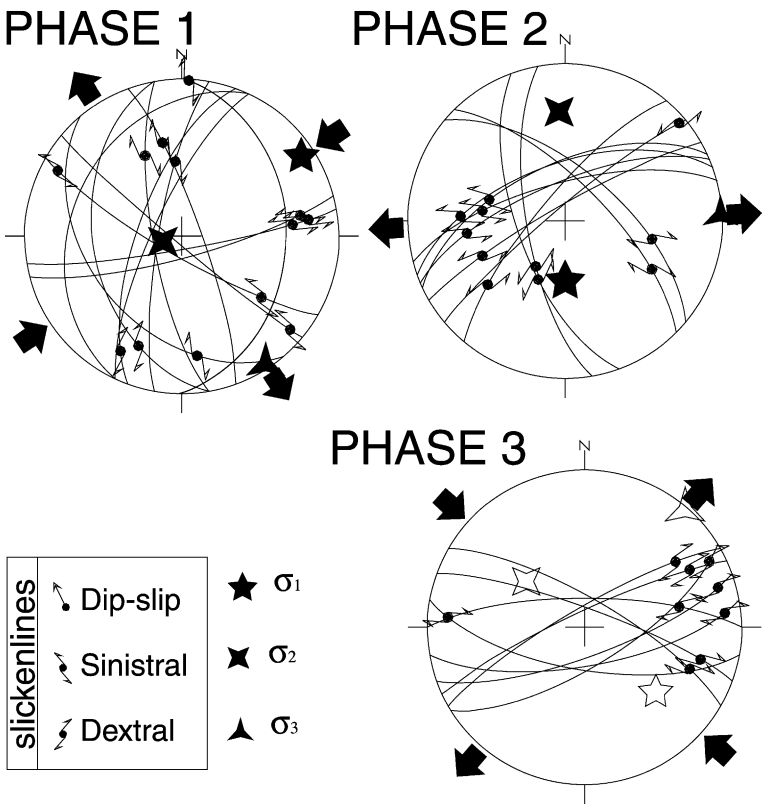

Fig. 10. Plots of fault planes, slickenlines and stress orientations for the whole data, in subarea 2, for each deformation phase (lower hemisphere, equal area projection).

namely, UTF 2 and UTF 3, could not be constrained precisely.

Along TGF 1 and TGF 2 (Tuğcu Faults), the NAOM has been thrusted over the Çandır Formation (a and b Fig. 11). In location c along the TGF 3, the NAOM is thrusted, towards the SW, over the Karabalçık Formation, and the Çandır Formation seals the thrust contact. This relation indicates that TGF 3 postdates the Early to Middle Eocene Karabalçk Formation, and predates the latest-Early Miocene to Middle Miocene (MN ?4–6) Çandır Formation.

The Karaçay Fault (KARF) is a NNE–SSW-oriented fault along which the Kocaçay Formation is thrusted over the İncik Formation. The thrust fault contact is sealed by the Çandır Formation in the south (location d in Fig. 11), and by the Tuğlu Formation in the north (location e in Fig. 11). This relation indicates that the thrusting predates the deposition of the Çandır Formation in the latest-Early Miocene to Middle Miocene (MN ?4–6) (see also Kaymakci et al., 2001a).

The Sağpazar Reverse Fault (SRF, Fig. 11) is observed between the overlying post-Middle Eocene to Oligocene Incik and the underlying Bozkır Formation. This relationship implies that the SRF postdates the deposition of the Bozkır Formation in latest-Late Miocene (MN-13) to Pliocene (Kaymakci et al., 2001a,b).

The Sungurlu Fault Zone is one of the largest structures in north Central Anatolia (Fig. 1). It is distributed over much of the study area and characterized by a number of generally NE–SW-striking faults that displace most of the above structures as well as the Late Miocene and Plio-Quaternary units (Deyim Formation). Along the master strand of the Sungurlu Fault Zone (MSFZ), the Gűvendik Syncline (GS) is rotated anticlockwise together with the Karaçay reverse Fault (KARF) implying sinistral activity on the

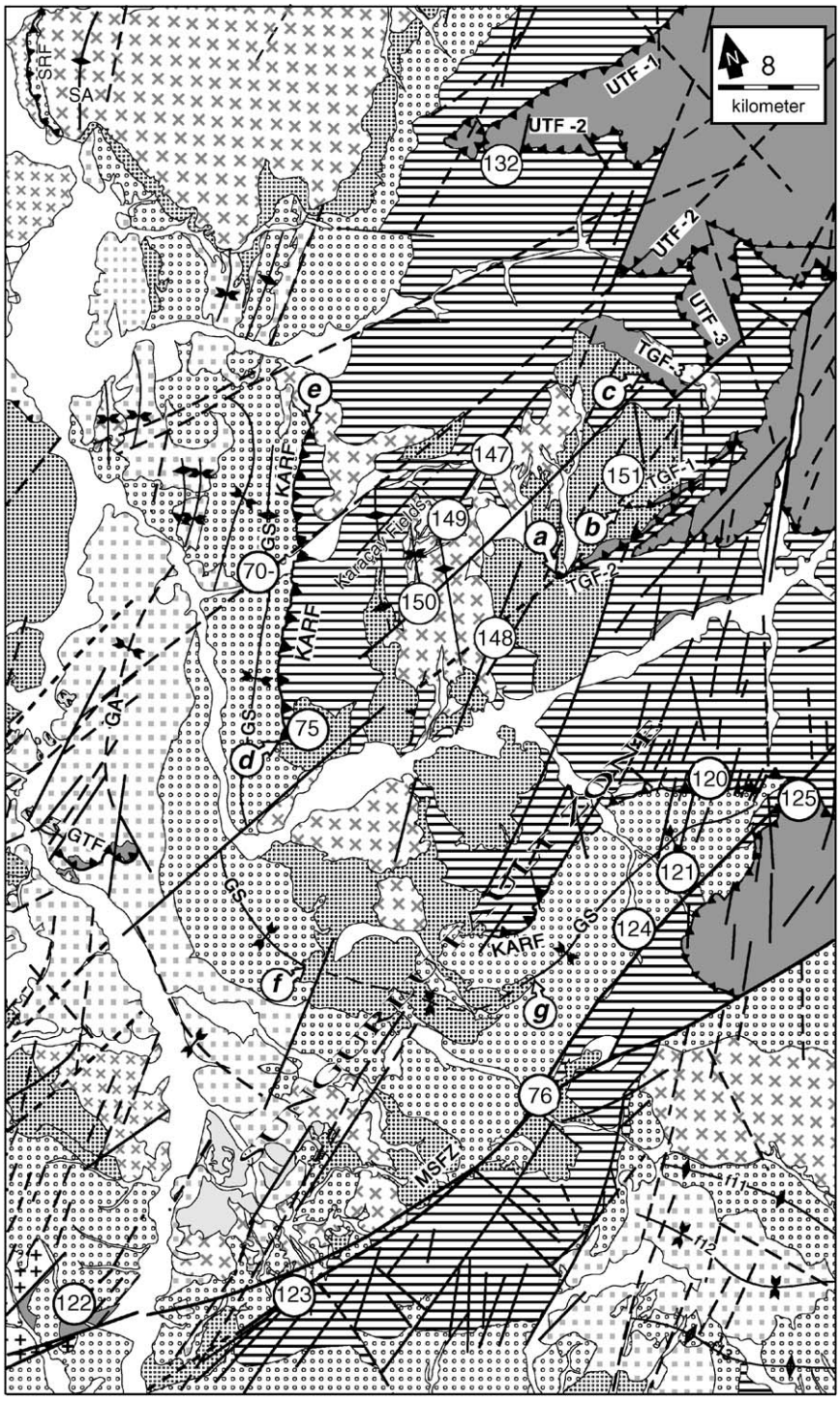

Fig. 11. Geological and sample location (site) map of subarea 3 (same legend as Fig. 4).

FAULTS							
Faults	hanging wall formations	foot wall formations	covering or youngest affected formations	dip range of the fault plane	possible age range	DEFORM. STYLE	AGE
NE-SW faults	Tuğlu & Süleymanlı	Tuğlu & Süleymanlı	Tuğlu and Süleymanlı (Late Miocene)	60˚-90˚	syn-to post Late Miocene	TRANSCURRENT	TORTONIAN TO RECENT
SRF	Incik	Süleymanl	Tuğlu and Süleymanlı (Late Miocene)	70˚-90˚	post-Late Miocene		
UTF 1&2	NAOM, Yalaçayı	Yoncalı Karabalçık Osmankahya	Yoncalı, Karabalçık and Osmankahya (Middle Eocene)	20˚-60˚	Early to Middle Eocene to recent		
UTF 3	NAOM, Yalaçayı, Yapraklı	Yoncalı Çandır	Yoncalı (Middle Eocene) and Çandır (Middle Miocene)	60˚	post-Middle Miocene		
TGF 1	NAOM	Karabalçık	Çandir (Middle Miocene)	60˚-90˚	syn- to Post-Middle Eocene, pre-Middle Miocene	TRANSPRESSION	PRE-MIDDLE MIOCENE
TGF 2	Dizilitaşlar	Yoncalı, Karabalçik	Yoncalı and Karabalçik (Middle Eocene)	60˚-90˚			
TGF 3	NAOM, Yalaçayı, Yapraklı	Karabalçık	Çandir (Middle Miocene)	70˚-90˚	Middle Eocene, pre-Middle Miocene		
KARF	Kocaçay	Incikı	Çandır (Middle Miocene) and Tuğlu (Late Miocene)	80˚	post-Middle Eocene pre-Middle Miocene		
GTF	NAOM	Gûvendik	Gûvendik (Oligocene)	30˚-50˚	post-mid-Oligocene pre-Middle Miocene		

FOLDS					
FOLDS	youngest folded unit	covering unit	dip range of axial plane	possible Compression direction	Age range
GS	Incik Güvendik	Çandır	30˚-70˚ (asymmetric)	WNW-ESE (NE-SW*)	syn- to post-mid-Oligocene pre-Middle Miocene
GA	Incik	Süleymanlı	60˚-80˚ (asymmetric)	WNW-ESE (NE-SW*)	
SA	Tuğlu	Deyim	80˚ (asymmetric)	E-W	post-Tortonian (MN10-12)
Karaçay folds	Tuğlu		80˚-90˚	E-W	

Fig. 12. Figure illustrating the structural characteristics, possible age ranges of the folds and faults developed in subarea 3. SRF: Sağpazar Reverse Fault, UTF: Uğurludağ Thrust Faults, TGF: Tuğcu Faults, KARF: Karaçay Reverse Fault, GTF: Gűvendik Thrust Fault, GS: Gűvendik Syncline, GA: Gűvendik Anticline, SA: Sağpazar Anticline.

Sungurlu Fault Zone, after the deposition of the Gűvendik Formation in the Oligocene (Kaymakci et al., 2001a,b; in press b). Along the subbranches of the Sungurlu Fault Zone, the Gűvendik Syncline (GS), the Karaçay Folds, the GTFs and the UTFs were displaced dextrally. The youngest dextrally displaced unit is the Messinian Bozkır Formation. These relationships indicate that the dextral Sungurlu Fault has been active since the Messinian (Kaymakci et al., 2001a).

4.3.2. Folds

The Gűvendik Syncline (GS) is developed within the post-Middle Eocene to Oligocene İncik and the Oligocene Gűvendik Formation. It is unconformably

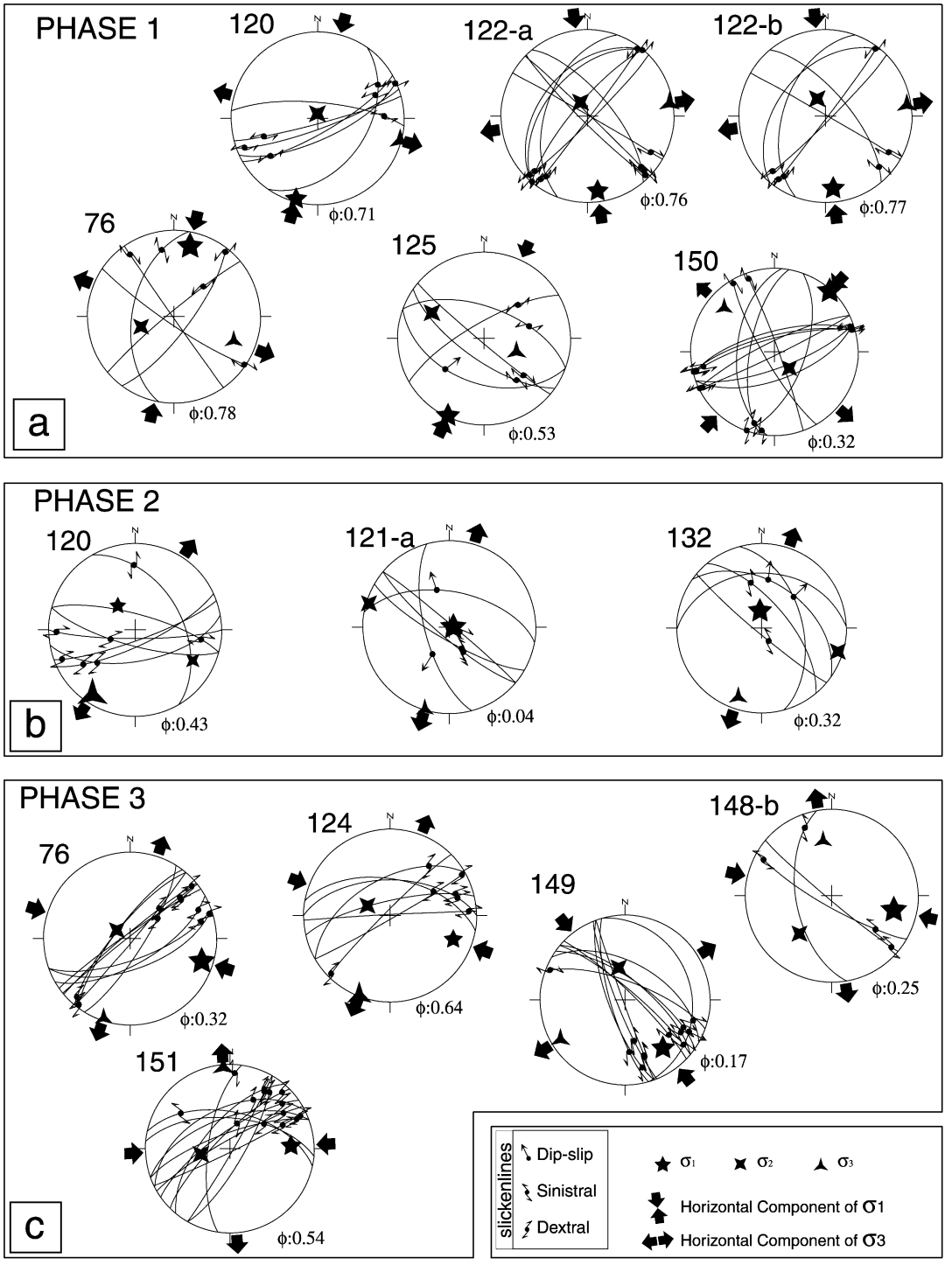

Fig. 13. Plots of faults planes, slickenlines, and stress orientations for each site in subarea 3 (lower hemisphere, equal area projection).

overlain by the latest-Early Miocene to Middle Miocene Çandır Formation (see f–g in Fig. 11). This relation indicates the post-Oligocene and pre-latest Early Miocene to Middle Miocene development of the GS after the Güvendik Formation and before the deposition of the Çandır Formation.

A number of folds are observed parallel to the Güvendik Syncline. They are developed within the Incik and Gűvendik Formations indicating their syn- to post-Oligocene development. In the NW part of the subarea they are covered by the Çandır and Tuğlu Formations indicating their pre-Middle Miocene development (Fig. 11).

The N–S-trending Karaçay Folds that are located around sites 148–150 are developed within the Tuğlu Formation, which indicates their post-Tortonian (MN 10–12) development related to an approximately E–W compression (Fig. 12).

The f11–f13 folds that developed in the SE corner of subarea 7 formed in the Incik and Güvendik Formations indicating their post-Oligocene origin.

4.3.3. Paleostress inversion

From 16 sites, 132 fault slip data were measured. One hundred sixteen of them were useful for the construction of paleostress tensors. The kinematic characteristics of each site in subarea 3 are summarized in Table 1. In sites 76 to 125, along all of the studied fault planes, three sets of overprinting calcite fibres were observed. The oldest set of calcite fibres indicates a sinistral movement for the NE–SW- to E–W-striking faults. The second set overprints the

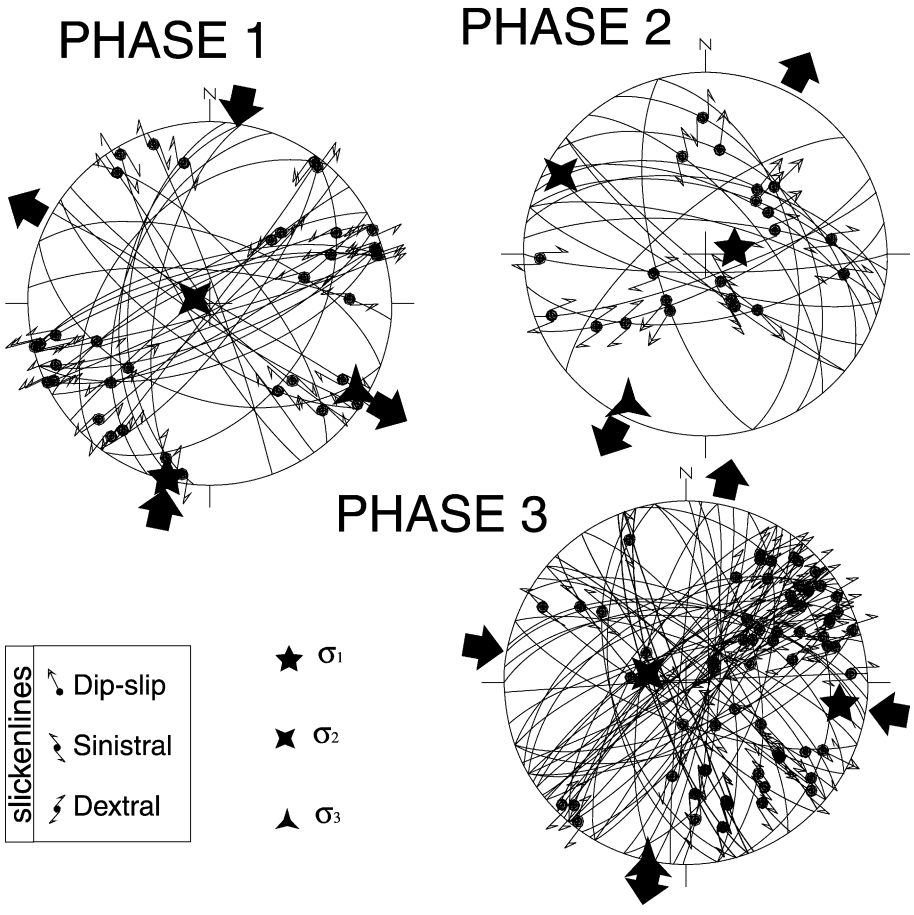

Fig. 14. Plots of fault planes, slickenlines and stress orientations for the whole data, in subarea 3, for each deformation phase (lower hemisphere, equal area projection).

abovementioned sinistral set. It generally displays a normal slip. The latest set overprints all the other sets. It exhibits dextral slip.

Phase 1: Six sites had sufficient data for the construction of site-based stress tensors (Fig. 13 and Table 2). The orientations of the principal stress axes were determined from strike-slip fault populations (76, 120, 122 and 150), which are relatively consistent. In all sites, except site 125, σ_2 is subvertical, σ_1 and σ_3 are subhorizontal. σ_1 varies between NNW–SSE to NE–SW. The mean orientations of stress for the subarea are as follows: $\sigma_1 = 199°N/03°$, $\sigma_2 = 306°N/80°$, $\sigma_3 = 109°N/10°$ (Fig. 14), in agreement with strike-slip regime. With σ_1 oriented NNE–SSW relative to NE–SW oriented faults would be left lateral (as reflected in the slip data) during this phase.

Phase 2: Three sites had sufficient data for the construction of the paleostress tensors in phase 2 (Fig. 13). In all sites, σ_1 is subvertical, σ_2, and σ_3 are subhorizontal and vary between WNW–ESE to NW–SE and NNE–SSW to NE–SW, respectively (Table 2). The orientations of the principal stress axes between sites and in the subarea-based orientations are relatively consistent. The orientations of the stress axes ($\sigma_1 = 080°N/77°$, $\sigma_2 = 299°N/10°$, $\sigma_3 = 207°N/08°$) show an extensional regime associated with a NNE–SSW-trending σ_3.

Phase 3: For this phase, we considered five sites with sufficient data for the paleostress reconstruction (Fig. 13). The orientation of the regional σ_1 is 100°N/23° with subvertical σ_2 and subhorizontal σ_3 (Fig. 14 and Table 2). In this strike-slip regime, NE–SW faults would work as right lateral as reflected in the fault slip data.

5. Discussion

5.1. Temporal relationships

The temporal relationships of the structures developed in the southern part of the Çankırı Basin are summarized in Figs. 5 and 12. Two different compression phases (deformation phases 1 and 3) separated by an extensional period (phase 2) have been determined using cross-cutting and unconformable relationships.

The cross-cutting relationships of the faults STF, KDF, BETF, KFZ, YFFZ, KFS, NE–SW-oriented faults, SRF, and UTF1 and UTF2 indicate regional transcurrent tectonics characterized by a transpressional and/or a transtensional component in the post-Middle Miocene. Based on the cross-cutting relationships and deformation styles of the Neogene units (Kaymakci et al., 2001a), the beginning of the regional transcurrent tectonics is circa Tortonian (MN 10–12, which corresponds approximately to 9.7 to 6.6 Ma).

The thrust faults and folds sealed by the Çandır Formation (Figs. 5 and 12) indicate a compressional tectonic regime prior to the regional transcurrent tectonics. The temporal relationships of some of these structures suggest that (1) the orientation of σ_1 in the earlier compressional regime is WNW–ESE and (2) a pre-latest-Early Miocene to Middle Miocene age. The growth fault patterns observed within the latest-Early Miocene to Middle Miocene (MN ?4–6) Çandır Formation, in the seismic sections (Kaymakci, 2000) and Neogene deformation styles Kaymakci et al. (2001a) also support that the earlier compressional phase ended prior to the deposition of the Çandır Formation.

Growth fault patterns, displacement of thrust faults by normal faults and inversion of some of these growth faults indicate that earlier compressional regime (phase 1) was superceded by an extensional regime (phase 2) in latest-Early Miocene to Middle Miocene (MN ?4–6, approximately 18.0 to 13.5 Ma; Kaymakci, 2000). This, in turn, was superceded (in the Late Miocene) by a new compressional regime characterized by regional transcurrent tectonics (phase 3) (Figs. 5 and 12, also Kaymakci et al., 2000, 2001a).

5.2. Correlation between the subareas

Phase 1: The trend of σ_1 varies from NNE–SSW to NE–SW in which a maximum deviation of 46° occurs between subareas 2 and 3 (Fig. 15b). The σ_2 is subvertical in each subarea whereas σ_1 and σ_3 are subhorizontal (strike-slip regime).

Paleomagnetic results have revealed that the western and southeastern parts of the Çankırı Basin have rotated anticlockwise between 27° and 36°, and the eastern margin has rotated 52° clockwise in the Early

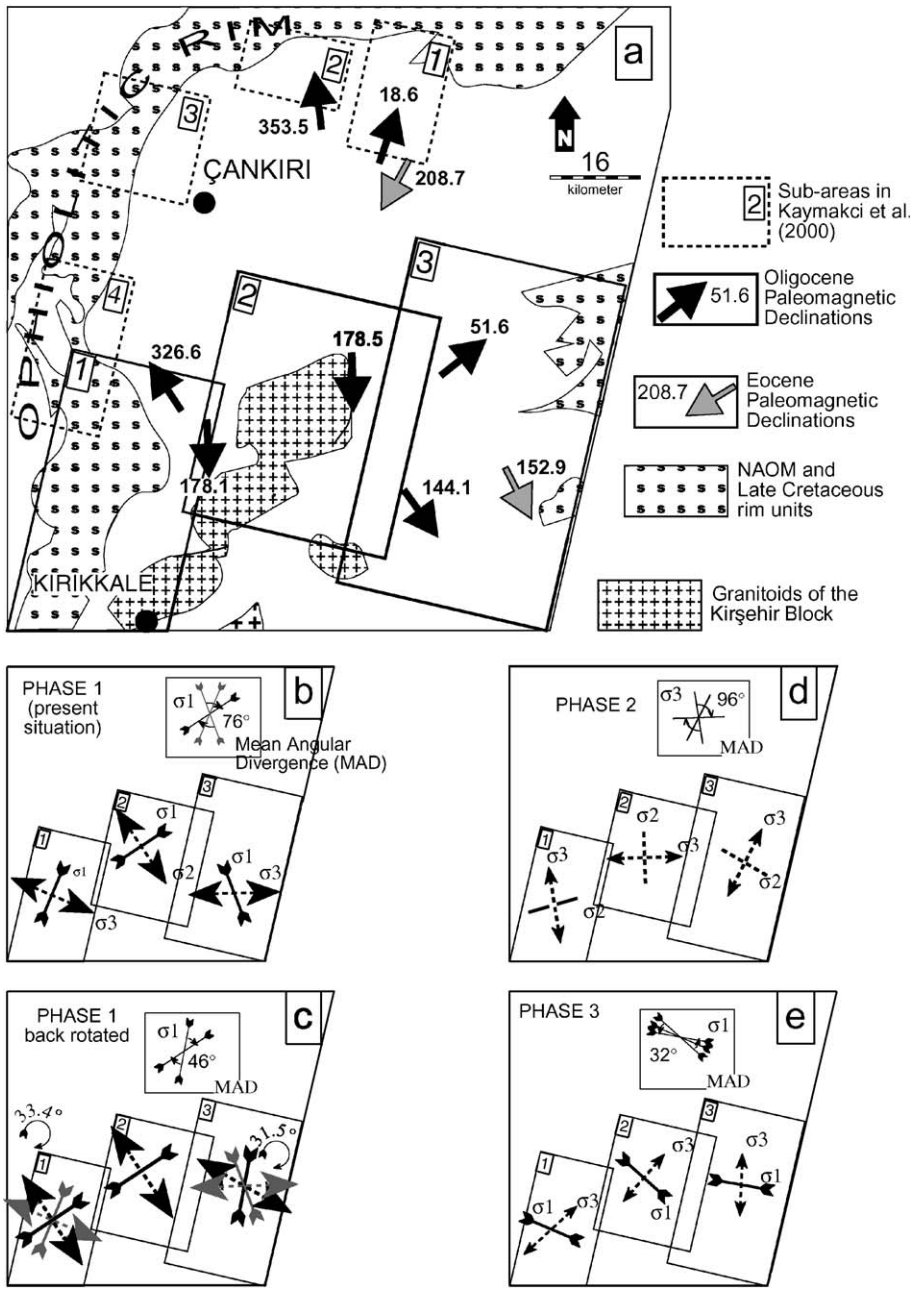

Fig. 15. (a) Simplified geological map illustrating the amount and orientations of paleodeclinations (see Kaymakci, 2000; Kaymakci et al., 2002). (b, d and e) Present-day horizontal component of the principal stress for each deformation phase. (c) Back rotated (rotation amounts are indicated) horizontal components of the principal stresses for phase 1 (present-day orientations are in gray). MAD: Maximum angular divergence between the stresses between subareas.

Eocene to pre-latest Early Miocene (Kaymakci, 2000; Kaymakci et al., in press b). The paleomagnetic declinations are illustrated in Fig. 15a. Because deformation phase 1 is thought to have occurred in the time range between the Early Eocene to pre-latest-Early Miocene (pre-Burdigalian), the paleostress data for this phase is restored according to the closest declination data. Therefore, the regional stress for subarea 1 is rotated clockwise (Fig. 15c). There is almost no rotation in the central part of the Çankırı Basin (i.e. subarea 2); therefore, no restoration was performed for this subarea for phase 1. The paleostress data for subarea 3 was collected from south of the YFFZ. Therefore, the regional stresses for this subarea were rotated clockwise (Fig. 15c), which is the average of the Eocene and Oligocene paleomagnetic declination

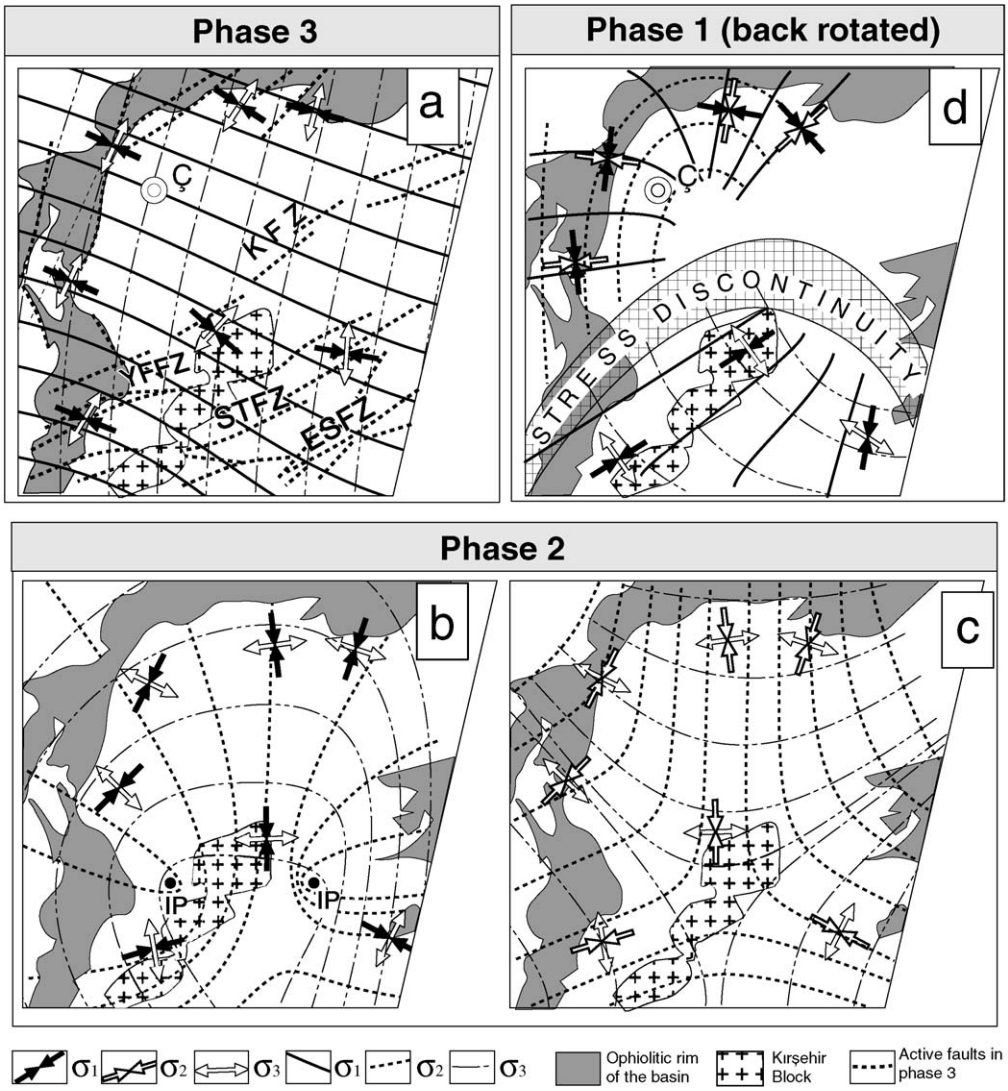

Fig. 16. Integrated smoothed trajectories of horizontal components of principal stress for each deformation phase. Ç: location of Çankırı town. Note that for the deformation phase 2, stress trajectory pattern given in 'b' is not feasible due to possibility of more than one isotropic points (IP) and orthogonality problem near the isotropic points, However, the pattern given in 'c' is more feasible and is more compatible with stress trajectories in the northern area (i.e. subareas 1–4 in Fig. 15).

data south of the YFFZ (Fig. 15a). Maximum angular divergence of σ_1 orientations between the subareas after back rotation becomes 76°.

Phase 2: This is a poor data set, but in all subareas, σ_1 is subvertical indicating an extensional regime. However, the horizontal component of σ_3 is poorly defined. It varies by as much as 96° (Fig. 15d).

Phase 3: In this phase (Fig. 15e) σ_1 is subhorizontal in all the subareas and the other stress axes are variable between the subareas. In subareas 2 and 3, σ_2 is subvertical while σ_3 is horizontal. However, in subarea 1, σ_3 is subvertical while σ_2 is subhorizontal. Maximum angular divergence in the horizontal component of σ_1 is 32° (Fig. 15e). With σ_1 trending WNW–ESE to NW–SE, the NE–SW-oriented strike-slip faults, namely, YFZ, STFZ, STFS, have reverse components in subarea 1. In the other subareas, σ_2 is subvertical indicating that the faults change their character from transpressional to transtensional from west (subarea 1) to east (mainly subarea 2) as their strikes change from NE–SW to E–W. This means that these faults form a restraining single bend in subarea 1 (Figs. 2, 6 and 8).

5.3. Stress trajectories

Stress trajectories are the representation of the variation of the paleostress pattern at regional scale. Mandl (1987) has discussed the existence and continuity of principal planes of stress that contain the principal stress axes (σ_1, σ_2, and σ_3). Treagus and Lisle (1997) have discussed and mathematically proved that planes of principal stresses are present and they are continuous if one of the principal stresses is constantly oriented, which means that the variation occurs only in two dimensions (see Ramsay and Lisle, 2000).

In relation to the Çankırı Basin, first the smoothed trajectories for the southern part of the Çankırı Basin have been plotted (subareas 1–3) using the constructed paleostress orientations discussed above, then the results were combined with the northern part of the Çankırı Basin discussed by Kaymakci et al. (2000). In plotting the trajectories, various combinations and patterns are possible. However, during plotting of the trajectories of the Çankırı Basin, as a whole, the smoothest pattern was aimed at bearing in mind that trajectories of one stress cannot cross each other. In this way, the number of possibilities for trajectory patterns is decreased.

Among the subareas, subarea 2 has few sites and slip data, which decreases the reliability of the results and hence the orientation of the stress trajectories. It should be kept in mind that as the new data become available this pattern might change only slightly. Nevertheless, subarea-based tensors combine all the data from individual sites, which increases the reliability of the results. In addition to this, agreement between paleostress and paleomagnetic results reinforces the confidence in the interpretations of both.

Phase 1: The horizontal component of the regional σ_1 orientation of phase 1 is relatively comparable to subareas 1 and 4 of Kaymakci et al. (2000). However, there is a conflict in the orientations of other stresses, such that σ_2 is subvertical in the southern part of the Çankırı Basin (subareas 1–3 of this study) while σ_3 is vertical in the north (Fig. 16a). This apparent conflict is interpreted as being due to the presence of different stress configurations in the same phase in different settings of the Çankırı Basin. It is interpreted that the configurations of the principal stresses in subareas 1–4 of Kaymakci et al. (2000) and 1–3 of this study are separated from each other along a possible stress discontinuity, which marks the interface between the basement (Kırşehir Block) and the fill of the Çankırı Basin. The σ_2 trajectories to the north of this dis-

Fig. 17. (a) Schematic structural map of the Çankırı Basin illustrating the relation between σ_1 and the type of structures (reactivated/inverted) in phase 3 (still active). MRF: Merzi Reverse Fault, ARF: Ayseki Reverse Fault, SA: Sağpazar Anticline, KFZ: Kızılırmak Fault Zone, EFZ: Eldivan Fault Zone, YFFZ: Yağbasan–Faraşlı Fault Zone, STFZ: Sivritepe Fault Zone, KFS: Kırıkkale Fault Set, MSFZ: Master Strand of the Sungurlu Fault Zone. (b) Riedel pattern of deformation and rose diagrams prepared from the lineaments of the Çankırı Basin (see Kaymakci, 2000) (see text for the discussion). (c) Sketch diagram illustrating the relationship between σ_1 and change of along strike kinematic characteristics of a dextral strike-slip fault (modified after Biddle and Christie-Blick, 1985). (d) Sketch diagram proposed for the patterns of faults and orientation of principal stresses during collision of an irregular indenter. Note thrusting in the front and transpressional deformation in the sides of the indenter. (e) Line drawings of thrust fault patterns developed in sandbox experiments (Zweigel, 1998). Note the geometry of the indenter and resultant pattern of the thrust faults. Note also the amounts along the displacement vectors, which are connecting the points from their pre-deformed and deformed positions.

continuity display a concentric pattern while σ_1 is radial. The center of the circles is located somewhere to the south of Çankırı town (Fig. 16a).

The trajectories to the south of the discontinuity display a mesh-like pattern with NNE–SSW- to NE–SW-oriented σ_1 and NW–SE-oriented σ_3, in which

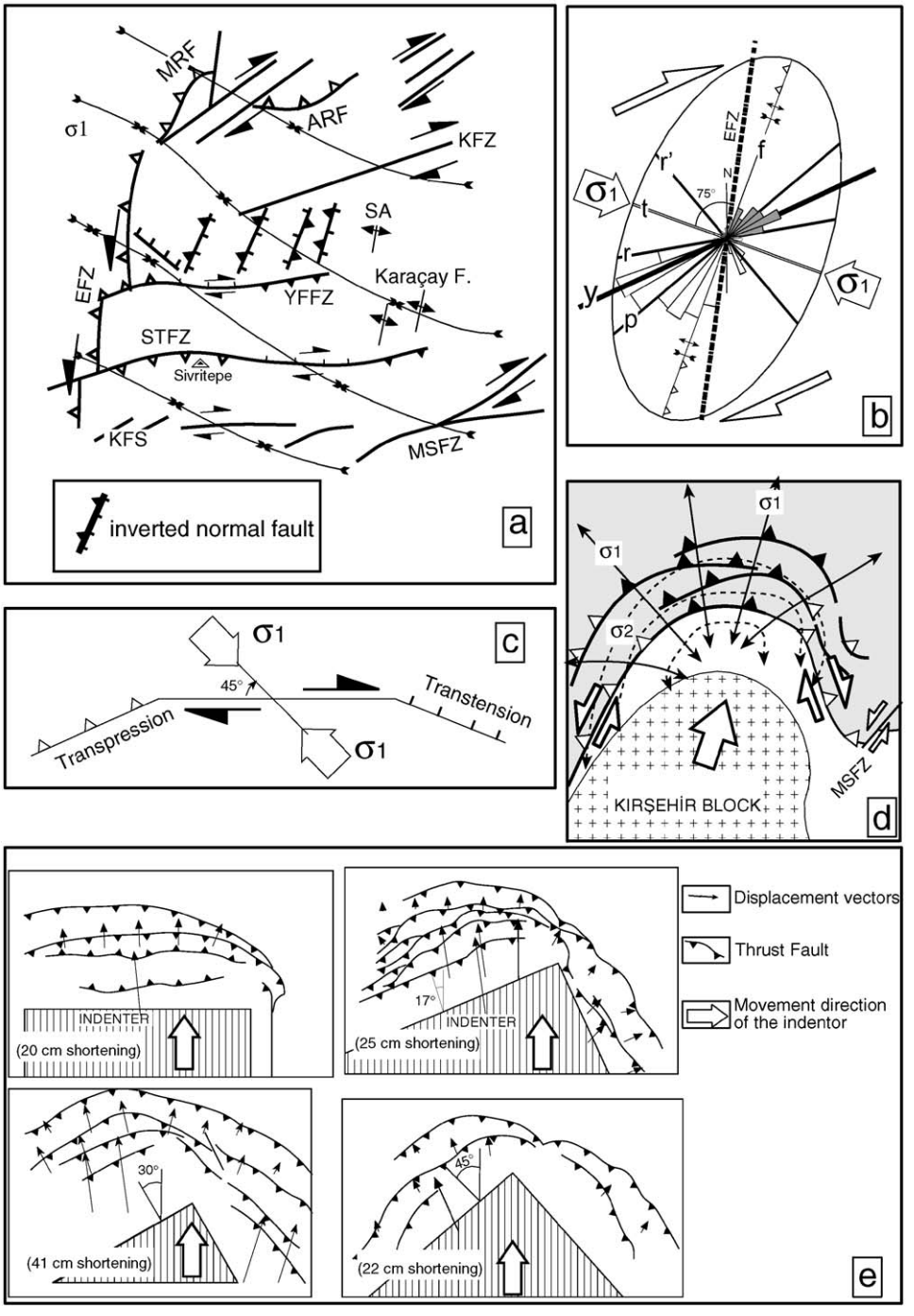

the σ_2 is vertical. This indicates predominance of strike-slip deformation in this part of the basin. σ_1 in subareas 1 and 2 are subparallel to the rim of the basin, while σ_3 is perpendicular to it. These relationships resemble the indentation tectonics (Tapponier et al., 1982) along an irregular margin (Zweigel, 1998). In such a model, the promontory of the Kırşehir Block serves as a partly rigid indenter. Areas in front (north) of the indenter were deformed by shortening and thrusting while the sides (western and eastern margin) of the indenter were characterized by transpression (Fig. 17e). The resultant deformation could explain the arcuate Ω-shape of the Çankırı Basin (Fig. 17d). The Sungurlu Fault Zone, during this deformation phase, might have accommodated the westward movement of the eastern margin of the basin via a sinistral movement (Fig. 17d).

Phase 2: Like phase 1, the stress trajectories of phase 2 integrate the paleostress data from Kaymakci et al. (2000). Phase 2 in this study corresponds to the phase 3 of Kaymakci et al. (2000). For deformation phase 2, two different patterns of stress trajectories are possible (Fig. 16b and c). One of the two constructed smoothed trajectories include two isotropic points (Fig. 16b), and close to these points the orthogonality of stress trajectories cannot be maintained (Fig. 16b). The compatible pattern has radial σ_3 trajectories with a subconcentric pattern about an axis located in subarea 2 (Fig. 16c). The elongations of the σ_3 trajectories are almost parallel to the present-day rim of the Çankırı Basin. This pattern of stress trajectories indicates almost uni-axial stress conditions in which the magnitudes of the horizontal stresses (σ_2 and σ_3) were close to, or equal to, each other with the vertical major compression (σ_1). Under such regimes high angle normal faults with an unconstrained strike directions develop. Therefore, they could have radial or multidirectional orientation (Carey and Brunier, 1974; Arlegui-Crespo and Simon Gomez, 1998). On the other hand, the approximately E–W elongation of the σ_3 trajectories in the central part of the Çankırı Basin implies preference for the faults to form in an approximately N–S direction (see Fig. 8), which would have high angle strike to the σ_3 trajectories.

Phase 3: Trajectories of the horizontal components of σ_1 and σ_3 for the last phase of deformation display a mesh-like pattern in which the σ_1 trajectory is oriented approximately WNW–ESE, and the σ_3 trajectories are oriented approximately NNE–SSW (Fig. 16d). In subarea 1, σ_3 is subvertical while in other subareas, both in the north and the south, σ_2 is vertical or subvertical. Subarea 1 is located within an area where NE–SW-oriented strike-slip faults, namely, YFFZ, STFZ, KFS, change their strike. They strike at a high angle to the σ_1 orientations and have a reverse component in this subarea (Fig. 17a).

The rose diagrams prepared from the lineaments of the Çankırı Basin display a Riedel pattern (Dresen, 1992; Kaymakci, 2000). The Kızılırmak, Sungurlu, Yağbasan–Faraşlı and Sivritepe Fault Zones are 30°–45° to σ_1 (Fig. 17a) and, therefore, represent y-shears in an idealized strain tensor (Fig. 17b). The faults that define the western margin of the Çankırı Basin (Eldivan Fault Zone—EFZ) make an angle of approximately 75° with σ_1 (f in Fig. 17b) and the subsequently inverted growth faults strike approximately perpendicular to σ_1 (Fig. 17a). Therefore, it is likely that the growth faults were inverted in phase 3 (Kaymakci, 2000). Because this phase is characterized by transcurrent tectonics, these faults may have sinistral lateral components which may be indicated by the late slickenlines with lateral components. In addition, one would expect that the mechanical properties of the basement, the basin fill and the basin rim were different. But the reconstructed stress trajectories are not deflected at the interfaces between basement, basin fill and the basin rim, although deflections in local scale (e.g. in individual sites) are possible. This implies that pre-existing structures and material properties did not play a major role in controlling the orientation of the principal stresses on regional scale (e.g. subarea scale). Near Sivritepe, and north of it, the angle between STF and YFFZ and the σ_1 trajectories increases. As previously mentioned, the fault zones in this area have a transpressional character (Fig. 17a and c). The σ_1 trajectories are also perpendicular to the Sağpazar Anticline (SA) and the Karaçay folds (Fig. 17a), which are parallel to the expected compressional structures in a Riedel system (f in Fig. 17b).

The orientations of the phase 3 σ_1 pattern are compatible with the present-day stress pattern of North Central Anatolia (Kaymakci, 2000). The Sungurlu Fault Zone and the Kızılırmak Fault Zones, two

splays of the North Anatolian Fault Zone, transferred transcurrent deformation into the Çankırı Basin area and displaced its rim, basement and the basin fill (Figs. 1 and 16a). The structures associated with this phase are formed in post-Middle Miocene rocks, implying it has been active since the middle of the Tortonian (i.e. MN 10–12, corresponding to 9.7 to 6.6 Ma).

5.4. Tectonic development of the Çankırı Basin

The information discussed above indicates that structural development of the Çankırı Basin occurred in four different tectonic regimes. The earliest phase is not well constrained and not detected in the southern part of the Çankırı Basin. The second phase (phase 1 of this study) is characterized by compressional deformation associated with transpression and was active in the pre-Burdigalian. The third phase is characterized by extensional deformation and was active in the post-Burdigalian to Late Miocene. The fourth phase is characterized by a regional transcurrent tectonics and has been active since the Late Miocene.

The last three deformation phases indicate that the evolution and structural development of southern part of the Çankırı Basin is accomplished first with indentation tectonics characterized by thrusting in its front and transpressional faulting in the sides of the indenter. It occurred in the Late Paleocene to pre-Burdigalian. Indentation continued until about the Early Miocene (Aquitanian). Then it was replaced by an extensional tectonic regime. The concentric pattern of the σ_3 trajectories and subvertical σ_1 indicates radial extension in the Middle Miocene after a period of contraction. Location of the pole of the σ_3 trajectories on the northern tip of the Kırşehir Block suggests that the extensional deformation is driven by the rebound of the tip of the block. This area is the locus of the Middle Miocene basaltic volcanic activity (Faraşlı Basalt, Fig. 3), which might have been related to a re-organization of the regional stress pattern to form a concentric pattern of σ_3 trajectories.

The extensional tectonic regime in the Middle Miocene is replaced by a regional transcurrent tectonic regime in the Late Miocene. In this phase, a number of ENE–WSW-oriented strike slip faults were developed. These faults are the splay faults of the right lateral North Anatolian Fault Zone and have dextral strike-slip sense (Kaymakci et al., 2000). These faults displaced the rim, the basement and the basin fill. The Sungurlu Fault Zone, which was a sinistral fault zone in the deformation phase 1, was reactivated as dextral strike-slip fault (compare Fig. 17a and d). The growth faults, which developed in the extensional period, were reactivated as reverse faults. In this phase, the Eldivan Fault Zone was reactivated in a sinistral sense (Fig. 17a). Almost no deflection of the stress trajectories occurred in the latest deformation phase, indicating that the pre-existing structures did not play a major role in the orientation of the principal stresses.

6. Conclusions

1. In the southern part of the Çankırı Basin, only three deformation phases are recognized. These phases correspond to the last three phases of the four phases recognized in the northern part of the Çankırı Basin.
   - Pre-Late Paleocene deformation regime (phase 1) is not detected in the southern part of the Çankırı Basin.
2. Late Paleocene to pre-Burdigalian transpression (phase 2) is characterized by subvertical σ_2 while other principal stresses were subhorizontal indicating a combination of transcurrent tectonics and thrusting (transpression). This phase lasted until about Aquitanien.
   - The northern and southern part of the Çankırı Basin have different stress configurations separated by a stress discontinuity, which is the interface of the Kırşehir Block and the basin in-fill. This discrepancy is interpreted as the change of the configuration of the stress ellipsoid due to the indentation of the Kırşehir Block into the Sakarya Continent.
3. Early to Middle Miocene extension (phase 3) is characterized by subvertical σ_1 and subhorizontal σ_3. It occurred in Burdigalian to pre-Tortonian.
   - The trajectories of the σ_3 display a concentric pattern, which is interpreted as the manifestation of radial extension.
4. The Late Miocene to Present regional transcurrent regime (phase 4) is characterized by subvertical σ_2

and subhorizontal σ_1. This phase has been active since the Tortonian.

- The σ_1 and σ_3 trajectories display a mesh-like pattern and are compatible with the current tectonic scheme of Turkey which is controlled mainly by the transcurrent North Anatolian Fault Zone.

Acknowledgements

The authors would like to thank Jacques Angelier and Ken Hardcastle for supplying their paleostress inversion software. Jacques Angelier, Richard Lisle and Aral Okay are thanked for reviewing the first draft of this paper. Yakup Ozcelik and Yurdal Öztaş are thanked for field guidance, assistance and fruitful discussions in the field camps. Turkish Petroleum is thanked for the field facilities. N.K. thanks Andrea Zanchi for introducing and teaching the handling of Angelier's software. Eric Barrier and Jim Granath are thanked for improving the English. N.K. is supported by the Kocaeli University (Turkey) YLS-grant.

References

Akyűrek, B., Bilginer, E., Akbaş, B., Hepşen, N., Pehlivan, S., Sunu, O., Soysal, Y., Dağer, Z., Çatal, E., Sőzeri, B., Yıldırım, H., Hakyemez, H., 1984. The geology of the Ankara–Elmadağ–Kalecik region. Chamb. Geol. Eng. Turk. Bull. 20, 31–46.

Angelier, J., 1979. Determination of the mean principal directions of stress for a given fault population. Tectonophysics 56, T17–T26.

Angelier, J., 1984. Tectonic analysis of fault slip data sets. J. Geophys. Res. 89, 5835–5848.

Angelier, J., 1994. Fault slip analysis and paleostress reconstruction. In: Hancock, P.L. (Ed.), Continental Deformation. Pergamon Press, Oxford, pp. 53–100.

Arlegui-Crespo, L.E., Simon Gomez, J.L., 1998. Reliability of paleostress analysis from fault striations in near multidirectional extension stress fields. Examples from the Ebro Basin, Spain. J. Struct. Geol. 20, 827–840.

Barka, A.A., Hancock, P.L., 1984. Neotectonic deformation patterns in the convex-northwards arc of the North Anatolian Fault Zone. In: Dixon, J.E., Robertson, A.H.F. (Eds.), The Geological Evolution of the Eastern Mediterranean. Spec. Publ. - Geol. Soc. Lond., vol. 17, pp. 763–774.

Biddle, K.T., Christie-Blick, N., 1985. Deformation and basin formation along strike-slip faults. In: Biddle, K.T., Christie-Blick, N. (Eds.), Strike-slip Deformation, Basin Formation and Sedimentation. Spec. Publ.- Soc. Econ. Paleont. Miner., vol. 37, pp. 1–45.

Bott, M.P.H., 1959. The mechanics of oblique-slip faulting. Geol. Mag. 96 (2), 109–117.

Carey, E., Brunier, B., 1974. Analyse théorique et numérique d'une modèle méchanique élémentaire appliqué a l'étude d'une population de failles. C.R. Acad. Sci., Paris. Ser. D 279, 891–894.

Dellaloğlu, A.A., Tűysűz, O., Kaya, O.H., Harput, B., 1992. Kalecik (Ankara)-Eldivan–Yapraklı (Çankırı)-İskilip (Çorum) ve Devrez Çayı arasindaki alanın jeolojisi ve petrol olanakları, TPAO Rap. No. 3194 (unpublished).

Doblas, M., 1998. Slickenside kinematic indicators. Tectonophysics 295, 187–197.

Dresen, G., 1992. Stress distribution and the orientation of Riedel shears. Tectonophysics 188, 239–247.

Etchecopar, A., Visseur, G., Daignieres, M., 1981. An inverse problem in microtectonics for the determination of stress tensors from fault striation analysis. J. Struct. Geol. 3, 51–65.

Gőrűr, N., Oktay, F.Y., Seymen, I., Şengőr, A.M.C., 1984. Palaeotectonic evolution of the Tuzgőlű basin complex, Central Turkey: sedimentary record of a neotethyan closure. In: Dixon, A.H.F., Robertson, A.H.F. (Eds.), The Geological Evolution of the Eastern Mediterranean. Blackwell Sci. Publ., Oxford. 824 pp.

Hancock, P.L., 1985. Brittle microtectonics: principles and practice. J. Struct. Geol. 7 (3/4), 437–457.

Hardcastle, K.C., 1989. Possible paleostress tensor configurations derived from fault-slip data in eastern Vermont and eastern New Hampshire. Tectonics 8 (2), 265–284.

Hardcastle, K.C., Hills, L.S., 1991. BRUTE3 and SELECT: QuickBasic 4 programs for determination of stress tensor configurations and separation of heterogeneous populations of fault-slip data. Comput. Geosci. 17, 23–43.

Kaymakci, N., 2000. Tectono-stratigraphical evolution of the Çankiri Basin (Central Anatolia, Turkey). Ph.D. Thesis, Utrecht University, The Netherlands. Geologica Ultraiectina, No. 190. 248 pp.

Kaymakci, N., Koçyiğit, A., 1995. Mechanism and basin generation in the splay fault zone of the North Anatolian Fault Zone: E.U.G. 8th. Conference on the Earth Sciences, Strasbourg. Abstract.

Kaymakci, N., White, S.H., van Dijk, P.M., 1998. Paleostress inversion in a multi-phase deformed area: Çankiri Basin (central Anatolia). 3rd International Turkish Geol. Symp.: Progress in Understanding the Geology of Turkey. 31 August–4 Sept. (1998) METU, Ankara, Turkey. Abstract.

Kaymakci, N., White, S.H., van Dijk, P.M., 2000. Paleostress inversion in a multi-phase deformed area: kinematic and structural evolution of the Cankiri Basin (central Turkey): Part 1. In: Bozkurt, E., Winchester, J.A., Piper, J. (Eds.), Tectonics and Magmatism in Turkey and its Surroundings. Spec. Publ. - Geol. Soc. Lond., vol. 173, pp. 445–473.

Kaymakci, N., Özçelik, Y., White, S.H., Van Dijk, P.M., 2001a. Neogene tectonic development of the Çankiri Basin (Central Anatolia, Turkey). Turk. Assoc. Pet. Geol. 13 (1), 27–56.

Kaymakci, N., de Bruijn, H., White, S.H., Unay, E., van Dijk, P.M., Sarac, G., 2001b. Implications of the Neogene stratigraphy of the Çankiri Basin. In: Guleç, E., Begun, D., Geraddds, D. (Eds.), Geology and Vertebrate Paleontology of the Middle Miocene Hominoid Locality Çandır (Central Anatolia, Turkey). CFS, Cour. Forsch.inst. Senckenb. Spec. Publ. In press.

Kaymakci, N., Duermeijer, C.E., Langereis, C., White, S.H., van Dijk, P.M., 2002. Paleomagnetic evolution of the Çankırı Basin (central Anatolia, Turkey): implications for oroclinal bending due to indentation. J. Geophys. Res. (submitted for publication).

Koçyiğit, A., 1989. Suşehri basin: an active fault-wedge basin on the North Anatolian Fault Zone, Turkey. Tectonophysics 167, 13–29.

Koçyiğit, A., Tűrkmenoğlu, A., Aksoy, E., Beyhan, A., Kaymakci, N., 1995. Post-collisional tectonics of Eskişehir–Ankara–Çankırı segment of İzmir–Ankara–Erzincan Suture Zone (IAESZ): Anakara Orogenic Phase. TPJD Bull. 6 (1), 69–86.

Krantz, R.W., 1988. Multiple fault sets and three-dimensional strain: theory and application. J. Struct. Geol. 10, 225–237.

Lisle, R.J., 1987. Principal stress orientations from faults: an additional constraint. Ann. Tecton. 1, 155–158.

Mandl, G., 1987. Discontinuous fault zones. J. Struct. Geol. 9, 105–110.

Means, W.D., 1987. A newly recognized type of slickenside striation. J. Struct. Geol. 9, 585–590.

Őzçelik, Y., 1994. Tectono-stratigraphy of the Laçin area (Çorum-Turkey). M.Sc. Thesis, METU. Geol. Eng. Dept. 133 pp. (unpublished).

Petit, J.-P., Laville, E., 1985. Morphology and microstructure of hydroplastic slickensides in sandstone. Program. Conference on Deformation Mechanisms in Sediments and Sedimentary Rocks. University College, London. Abstract.

Pollard, D.D., Saltzer, S.D., Rubin, A.M., 1993. Stress inversion methods: are they based on faulty assumptions? J. Struct. Geol. 15 (8), 145–154.

Ramsay, J.G., Lisle, R.J., 2000. Applications of continuum mechanics in structural Geology. Modern Structural Geology, vol. 3. Academic Press, London, pp. 702–717.

Reches, Z., 1987. Determination of the tectonic stress tensor from slip along faults that obey the Coloumb yield criterion. Tectonics 6, 849–861.

Şengőr, A.M.C., Yılmaz, Y., 1981. Tethyan evolution of Turkey: a plate tectonic approach. Tectonophysics 75, 181–241.

Şengőr, A.M.C., Yılmaz, Y., Sungurlu, O., 1984. Tectonics of the Mediterranean Cimmerides: nature and evolution of the western termination of palaeo-Tethys. In: Dixon, J.E., Robertson, A.H.F. (Eds.), The Geological Evolution of the Eastern Mediterranean. Spec. Publ. - Geol. Soc. Lond., vol. 17, pp. 77–112.

Şengőr, A.M.C., Şaroğlu, F., Gőrűr, N., 1985. Strike-slip deformation and related basin formation in zones of tectonic escape: Turkey as a case study. In: Biddle, K.T., Christie-Blick, N. (Eds.), Strike-slip Deformation Basin Formation and Sedimentation. Spec. Publ. - Soc. Econ. Palaeo. Miner., vol. 37, pp. 227–264.

Tapponier, P., Peltzer, G., Le Dain, A.Y., Armijo, R., Cobbold, P., 1982. Propagating extrusion tectonics in Asia: new insights from simple experiments with plasticine. Geology 10, 611–616.

Treagus, S.H., Lisle, R., 1997. Do principal surfaces of stress and strain always exist? J. Struct. Geol. 19, 997–1010.

Tűysűz, O., Dellaloğlu, A.A., 1992. Çankırı Havzasının Tektonik birlikleri ve jeolojik evrimi. Tűrkiye 9. Petrol Kongr. Bildir. Kitabı, 333–349.

Twiss, R.J., Unruh, J.R., 1998. Analysis of fault slip inversion; do they constrain stress or strain rate? J. Geophys. Res. 103 (B6), 12205–12222.

Wallace, R.E., 1951. Geometry of shearing stress and relation to faulting. J. Geol. 69, 118–130.

Wojtal, S., Pershing, J., 1991. Paleostress associated with faults of large offset. J. Struct. Geol. 13, 49–62.

Zweigel, P., 1998. Arcuate accretionary wedge formation at convex plate margin corners: results of sandbox analogue experiments. J. Struct. Geol. 20, 1597–1609.